

3 mm Spectroscopic Observations of Massive Star-Forming Regions with IRAM 30-m

Xuefang Xu^{1,2}, Junzhi Wang³, Qian Gou^{1,2}, Juan Li^{4,5}, Donghui Quan⁶, Di Li^{7,8}, Fei Li⁹, Chunguo Duan¹, and Juncheng Lei¹

¹School of Chemistry and Chemical Engineering, Chongqing University, Chongqing 401331, China

²Chongqing Key Laboratory of Chemical Theory and Mechanism, Chongqing 401331, China

³Guangxi Key Laboratory for Relativistic Astrophysics, Department of Physics, Guangxi University, Nanning 530004, China

⁴Shanghai Astronomical Observatory, Chinese Academy of Sciences, 80 Nandan Road, Shanghai 200030, China

⁵Key Laboratory of Radio Astronomy, Chinese Academy of Sciences, China

⁶Research Center for Intelligent Computing Platforms, Zhejiang Laboratory, Hangzhou 311100, China

⁷Department of Astronomy, Tsinghua University, Beijing 100084, China

⁸National Astronomical Observatories, Chinese Academy of Sciences, Beijing 100012, China

⁹School of Astronomy and Space Science, Nanjing University, Nanjing 210093, China

*E-mail: junzhiwang@gxu.edu.cn, qian.gou@cqu.edu.cn

Received (reception date); Accepted (acceptation date)

Abstract

Broadband spectroscopic observations with high sensitivity provide an unbiased way to detect emissions of molecules in space. We present deep observations from 105.8 GHz to 113.6 GHz toward 50 Galactic massive star-forming regions using IRAM 30-m millimeter telescope, with noise levels ranging from 6 to 29 mK at frequency channel spacing of 195 kHz, which corresponds to $\sim 0.54 \text{ km s}^{-1}$ at 110 GHz. Totally, 27 molecular species have been identified, of which 16 are complex organic molecules. The related parameters, such as peak temperature, integrated intensity, and line width of the identified molecular lines were obtained. The line widths of the chemically related molecules show strong positive correlations, suggesting they likely originate from similar gases within star-forming regions. This work highlights the fundamental properties of the detected molecular lines and offers a valuable dataset for further studies on the astrochemical evolution of molecules in massive star-forming cores.

Key words: key word *astrochemistry*₁ — key word *line : identification*₂ — key word *ISM : clouds*₃ — ... — key word *ISM : molecules*₄

1 Introduction

Massive star-forming regions, the cradles of high mass stars ($M > 8 M_{\odot}$), are one kind of the most chemically rich sources in the Milky Way (Schilke et al. 1997; Gibb et al. 2000; Belloche et al. 2013; Belloche et al. 2017; Belloche

et al. 2019). Information on the chemical condition of different massive star-forming regions would advance our understanding of the high-mass star formation (Remijan et al. 2003; Motte et al. 2018; van der Walt et al. 2021). For example, Orion KL (Tercero et al. 2011; Feng et al. 2015; Bernal et al. 2021; Wilkins et al. 2022) and Sgr

B2 (Bonfand et al. 2019; Li et al. 2021; Kolesniková et al. 2022), where approximately 90% detected interstellar molecules were first observed, have been found to be natural laboratories for the inventory and formation mechanism of molecules. Besides, other massive star-forming regions at different stages, such as W3(H₂O), W3(OH), W33A, W43, W51, W75N, ON1, Cep E, AFGL2591, have been conducted with molecular censuses and investigated possible formation pathways of molecules (van der Tak et al. 2000; Fontani et al. 2007; Foster et al. 2011; Vasyunina et al. 2014; Coletta et al. 2020). However, the abundances of most complex molecules in interstellar space continue to challenge current understanding. These complexities cannot be fully explained by existing chemical models, which include standard processes, such as ion-molecule and electron recombination reactions, along with surface chemistry (Ceccarelli et al. 2023). Even the ubiquitous molecule methanol presents a challenge. To achieve a comprehensive understanding of interstellar chemistry, it is essential to test chemical models against observations.

Broadband spectroscopic observations with high sensitivity provide an effective way to obtain the chemical composition of a particular region (Bonfand et al. 2019; Jørgensen, Belloche & Garrod 2020), from which chemical models can be then tested and further improved. Rather than targeted searches with high-priority, broadband observations are unbiased and self-consistent in determining the true compositions of interstellar clouds by allowing the acquisition of spectral data over large frequency ranges and sample many transitions of each molecule (Kolesniková et al. 2022). Radio astronomical observatories, such as IRAM 30-m (Institute de Radioastronomie Millimétrique), Yebes 40m, ALMA (Atacama Large Millimeter/submillimeter Array), lead to a dramatic increase in the number of publicly available broadband spectroscopic observations of various sources, for example, low- and high-mass star-forming regions, the envelope of carbon-rich star (Cernicharo et al. 2022; Margulès et al. 2022; Qin et al. 2022; Pardo et al. 2022). The analysis and interpretation of these spectra are important goals in the field of astrochemistry.

In the present work, we focused on the identification of molecular species in 50 massive star-forming regions using IRAM’s spectroscopic observations between 105.8 and 113.6 GHz. In particular, among the 50 target sources, 25 sources (marked by † in Table 1) have not been conducted with spectroscopic observations before, which provides new data to gain more comprehensive view of their possible chemical and physical parameters. Weeds (Maret et al. 2011) was used to identify molecular species for our spectroscopic observations. This paper is organized as follows. Section 2 presents the spectroscopic observations

and detailed data reduction. The detected 30 species and radio recombination lines in our sample, and notes for individual sources are showed in Section 3. Section 4 is the discussion. The main results are summarized in Section 5.

2 Observations and data reduction

2.1 Observations

Broadband spectroscopic observations of 50 massive star-forming regions selected from Reid et al. (2014) were conducted with the IRAM 30-m millimeter telescope at Pico Veleta, Spain, on June and October 2016, and August 2017. The criteria to select the target sources were detailed in Li et al. (2022). The data used in this paper was taken by the 3 mm (E0) band of the Eight Mixer Receiver (EMIR). The Fourier Transform Spectrometers (FTS) cover 8 GHz bandwidth and provide a spectral resolution of 195 kHz (0.54 km s⁻¹) with dual polarization. Standard position switching mode with azimuth off of -600'' was adopted. Due to the emission at off position, the contamination can cause under-estimation for some strong lines with low critical density, which needs to be taken care only in sources like Sgr B2. Even for Sgr B2, it will be not important for most of the weak lines with high critical densities (Jones et al. 2012). Detailed descriptions of the observations were presented in Li et al. (2022). Table 1 lists the information of the 50 massive star-forming regions.

2.2 Data reduction

The data reduction was conducted with the GILDAS (Grenoble Image and Line Data Analysis Software) software package¹, including ‘CLASS’ (Continuum and Line Analysis Single-dish Software), ‘GREG’(Grenoble Graphic), and ‘Weeds’Maret:11. Main steps of data reduction are described as follows. We first averaged the scans of spectra for the same source after checking data quality of every scan. Less than 0.5% data were discarded due to poor baseline or bad channels. The first-order baseline was then applied on the averaged spectra for most of sources. Seven sources (G009.62+00.19, G010.47+00.02, G035.20–01.73, G059.78+00.06, G069.54–00.97, G081.75+00.59, and G081.87+00.78) were applied second-order baseline for the appearance of the significant break. Since G043.16+00.01 and G049.48–00.36 show regular small standing waves, they were subtracted sine baselines. The full scan of G009.62+00.19 after subtracting second order baselines is shown in Figure 1 (a) and (b). The observed lines in

¹ <http://www.iram.fr/IRAMFR/GILDAS>

Table 1. Properties of high-mass star forming regions.

Source	Alias	R.A.	Dec.	RMS	On-source	V_{sys}	D
(1)	(2)	(hh:mm:ss)	(dd:mm:ss)	(mK)	time (minutes)	(km s^{-1})	(k pc)
		(3)	(4)	(5)	(6)	(7)	(8)
G000.67−00.03	Sgr B2	17:47:20.00	−28:22:40.0	29	5.7	62	0.2
G005.88−00.39		18:00:30.31	−24:04:04.5	26	5.7	9	5.3
†G009.62+00.19		18:06:14.66	−20:31:31.7	19	11.3	2	3.3
G010.47+00.02		18:08:38.23	−19:51:50.3	19	11.3	69	1.6
G010.62−00.38	W31	18:10:28.55	−19:55:48.6	23	8.5	−3	3.8
†G011.49−01.48		18:16:22.13	−19:41:27.2	25	5.7	11	7.1
†G011.91−00.61		18:13:58.12	−18:54:20.3	14	11.3	37	5.1
†G012.80−00.20		18:14:14.23	−17:55:40.5	16	11.3	34	5.5
G012.88+00.48	IRAS 18089−1732	18:11:51.42	−17:31:29.0	14	11.3	31	5.9
†G012.90−00.24		18:14:34.42	−17:51:51.9	25	5.7	36	5.9
†G012.90−00.26		18:14:39.57	−17:52:00.4	18	8.5	39	5.9
†G014.33−00.64		18:18:54.67	−16:47:50.3	27	5.7	22	7.2
G015.03−00.67	M17	18:20:24.81	−16:11:35.3	19	5.7	22	6.4
†G016.58−00.05		18:21:09.08	−14:31:48.8	16	8.5	60	5.0
†G023.00−00.41		18:34:40.20	−09:00:37.0	14	11.3	80	4.5
†G023.44−00.18		18:34:39.19	−08:31:25.4	14	11.3	97	3.7
†G027.36−00.16		18:41:51.06	−05:01:43.4	13	11.3	92	3.9
†G028.86+00.06		18:43:46.22	−03:35:29.6	12	11.3	100	4.0
G029.95−00.01	W43S	18:46:03.74	−02:39:22.3	18	11.3	98	4.6
†G031.28+00.06		18:48:12.39	−01:26:30.7	17	11.3	109	5.2
G031.58+00.07	W43Main	18:48:41.68	−01:09:59.0	15	11.3	96	4.9
†G032.04+00.05		18:49:36.58	−00:45:46.9	10	19.8	97	4.8
†G034.39+00.22		18:53:18.77	+01:24:08.8	8	39.0	57	7.1
†G035.02+00.34		18:54:00.67	+02:01:19.2	8	39.0	52	6.5
†G035.19−00.74		18:58:13.05	+01:40:35.7	13	14.1	30	6.6
†G035.20−01.73		19:01:45.54	+01:13:32.5	10	22.6	42	5.9
†G037.43+01.51		18:54:14.35	+04:41:41.7	9	34.5	41	6.9
G043.16+00.01	W49N	19:10:13.41	+09:06:12.8	14	19.8	10	7.6
G043.79−00.12	OH 43.8−0.1	19:11:53.99	+09:35:50.3	10	25.5	44	5.7
G049.48−00.36	W51 IRS2	19:23:39.82	+14:31:05.0	15	11.3	56	6.3
G049.48−00.38	W51M	19:23:43.87	+14:30:29.5	12	11.3	58	6.3
†G059.78+00.06		19:43:11.25	+23:44:03.3	11	14.1	25	7.5
G069.54−00.97	ON1	20:10:09.07	+31:31:36.0	10	22.6	12	7.8
†G075.76+00.33		20:21:41.09	+37:25:29.3	8	22.6	−9	8.2
G078.12+03.63	IRAS 20126+4104	20:14:26.07	+41:13:32.7	16	11.3	−4	8.1
G081.75+00.59	DR21	20:39:01.99	+42:24:59.3	9	22.6	−3	8.2
G081.87+00.78	W75N	20:38:36.43	+42:37:34.8	11	19.8	7	8.2
†G092.67+03.07		21:09:21.73	+52:22:37.1	12	14.1	−5	8.5
G109.87+02.11	Cep A	22:56:18.10	+62:01:49.5	10	22.6	−7	8.6
G111.54+00.77	NGC 7538	23:13:45.36	+61:28:10.6	6	85.5	−57	9.6
G121.29+00.65	L1287	00:36:47.35	+63:29:02.2	6	60.0	−23	8.8
G123.06−06.30	NGC281	00:52:24.70	+56:33:50.5	8	64.5	−30	10.1
G133.94+01.06	W3OH	02:27:03.82	+61:52:25.2	13	11.3	−47	9.8
G168.06+00.82	IRAS 05137+3919	05:17:13.74	+39:22:19.9	17	14.1	−27	15.9
†G176.51+00.20		05:37:52.14	+32:00:03.9	6	117.0	−17	9.3
†G183.72−03.66		05:40:24.23	+23:50:54.7	5	87.0	3	10.0
G188.94+00.88	S 252	06:08:53.35	+21:38:28.7	9	60.0	8	10.4
G192.60−00.04	S 255	06:12:54.02	+17:59:23.3	9	57.0	6	9.9
G209.00−19.38	Orion Nebula	05:35:15.80	−05:23:14.1	6	84.0	3	8.6
†G232.62+00.99		07:32:09.78	−16:58:12.8	8	75.0	21	9.4

Note. † Sources have not been conducted with spectroscopic observations before. Columns (1) and (2) give the Galactic source name/coordinates and an alias, when appropriate. Right Ascension and Declination (J2000) are listed in columns (3) and (4). Columns (5), (6), (7), and (8) list RMS, on-source time, systemic velocities and distances of sources from the galactic centre, respectively. Values in columns (7) and (8) are taken from Reid et al. (2014) and Li et al. (2022), respectively.

each source were then identified using Weeds. The line identification relied heavily on the accuracy of frequencies and line strengths derived from the analysis of laboratory measurements. Weeds was also used to model the synthetic spectra of the observed lines with the assumption of local thermodynamic equilibrium (LTE). The JPL (Jet Propulsion Laboratory) (Pickett et al. 1998) and CDMS (Cologne Database for Molecular Spectroscopy) (Müller et al. 2005; Endres et al. 2016) molecular databases were used for the whole identification and spectral modeling process. Spectral modeling is supported by five parameters: source size, rotational temperature (Col. (3) in Table 2), column density (Col. (4) in Table 2), velocity offset (Col. (5) in Table 2) with respect to the systemic velocity (Col. (7) in Table 1), and line width. To standardize our analysis across different distances, a uniform source size of $10''$ was applied to all observed sources. This assumption is

based on typical extents of emission in similar studies (Li et al. 2022), which suggests a reasonable compromise between resolution limits (the angular resolution, $\sim 24''$, of the IRAM data) and actual source sizes. This approach introduces an estimated uncertainty of about 30% in our column density calculations. However, the provided parameters, including line intensities and widths in each source, do not significantly change with different assumed source sizes. Figure 1 (c) is an example for the modeling synthetic spectrum (red solid line) overlaid with the observed lines in G009.62+00.19. Finally, Gaussian fits were performed for the identified lines to get peak intensity, centroid velocity, full width at half maximum (FWHM), and integrated intensity. The results derived with Gaussian fitting are reported in Section 3.1.

Table 2. Rotational temperatures and column densities of detected molecules using in Weeds

Source	Species	Rotational Temperature (K)	Column Density (cm^{-2})	Velocity offset (km s^{-1})	Source	Species	Rotational Temperature (K)	Column Density (cm^{-2})	Velocity offset (km s^{-1})		
(1)	(2)	(3)	(4)	(5)	(1)	(2)	(3)	(4)	(5)		
G000.67−00.03	NH ₂ CHO	45	1.8×10^{15}	0.2	G035.02+00.34	CCS	45	2.0×10^{13}	1.0		
	CCS	45	2.5×10^{14}	0.5		HC ₅ N	45	1.5×10^{13}	1.0		
	C ₂ H ₅ CN	45	2.0×10^{14}	0.		³⁴ S ₂ O	45	3.7×10^{13}	-0.5		
	HC ₅ N	45	8.5×10^{13}	0.		CH ₃ OH	85	2.2×10^{15}	0.		
	C ₂ H ₃ CN	45	8.0×10^{14}	0.5		t-HCOOH	85	1.2×10^{14}	1.0		
	C ₂ H ₅ OH	45	3.5×10^{15}	0.		¹³ CN	85	1.0×10^{14}	1.0		
	CH ₃ OCH ₃	45	9.0×10^{15}	0.		HC ₃ N	85	3.0×10^{14}	1.0		
	OC ³⁴ S	45	1.5×10^{15}	0.		SO	45	1.5×10^{15}	0.5		
	CH ₃ OH	45	3.3×10^{16}	-2.0		OCS	45	4.7×10^{14}	0.5		
	CH ₃ C ¹⁵ N	45	8.5×10^{13}	-2.0		C ¹⁸ O	85	2.2×10^{17}	0.		
	¹³ CH ₃ CN	45	1.0×10^{14}	0.		HNCO	45	7.5×10^{13}	1.0		
	CH ₃ SH	45	4.5×10^{15}	0.		¹³ CO	85	1.7×10^{18}	0.		
	CH ₃ OCHO	45	1.0×10^{16}	0.		CH ₃ CN	45	3.8×10^{13}	0.		
	SO ₂	45	1.6×10^{16}	-2.0		CH ₃ CHO	45	1.7×10^{14}	0.		
	t-HCOOH	45	1.5×10^{15}	0.		C ¹⁷ O	45	3.3×10^{16}	0.2		
	SiS	45	9.0×10^{14}	0.		CN	45	3.5×10^{15}	1.0		
	HC ₃ N	45	4.0×10^{15}	0.		G035.19−00.74	NH ₂ CHO	45	2.3×10^{13}	3.0	
	SO	45	1.2×10^{16}	0.			CCS	45	2.7×10^{13}	4.0	
	HC ₃ N, $\nu_7=1$	45	1.0×10^{17}	0.			HC ₅ N	45	2.2×10^{13}	4.5	
	OCS	45	1.3×10^{16}	0.			³⁴ S ₂ O	45	4.5×10^{13}	2.0	
	HNCO	45	1.2×10^{15}	0.			CH ₃ OCH ₃	45	1.5×10^{15}	2.0	
	C ¹⁸ O	45	5.1×10^{17}	3.0			OC ³⁴ S	45	1.0×10^{14}	2.0	
	¹³ CO	85	8.0×10^{18}	3.0			CH ₃ OH	85	2.7×10^{16}	1.5	
	CH ₃ ¹³ CN	45	1.2×10^{14}	0.			CH ₃ OCHO	85	1.2×10^{15}	3.0	
	CH ₃ CN	45	1.5×10^{15}	0.			SO ₂	85	1.7×10^{15}	1.0	
	CH ₃ CHO	45	2.6×10^{15}	0.			t-HCOOH	85	3.0×10^{14}	4.0	
	C ¹⁷ O	45	1.6×10^{17}	3.5			¹³ CN	85	2.0×10^{14}	4.0	
	CN	85	1.0×10^{15}	-2.0			HC ₃ N	85	6.0×10^{14}	4.0	
	G005.88−00.39	CCS	45	5.2×10^{13}			0.	SO	45	1.8×10^{15}	4.0
		HC ₅ N	45	9.5×10^{13}			-0.5	OCS	45	1.3×10^{15}	4.0
		C ₂ H ₃ CN	45	1.1×10^{14}			-0.5	C ¹⁸ O	85	2.0×10^{17}	4.0
		CH ₃ OH	45	6.5×10^{15}		0.5	HNCO	45	2.5×10^{14}	4.0	
		SO ₂	45	1.0×10^{18}		0.	C ¹⁵ N	45	3.0×10^{13}	4.0	
		CH ₃ C ₃ N	45	7.0×10^{13}		0.	¹³ CO	85	3.0×10^{18}	4.0	
		¹³ CN	45	3.2×10^{14}		-0.7	CH ₃ CN	45	1.7×10^{14}	3.5	
HC ₃ N		85	8.5×10^{15}	0.	CH ₃ CHO	45	5.2×10^{14}	4.0			
SO		45	1.0×10^{16}	0.	C ¹⁷ O	45	2.3×10^{16}	4.0			
HC ₃ N, $\nu_7=1$		85	1.5×10^{15}	0.5	CN	45	3.0×10^{15}	4.0			
OCS		45	3.0×10^{15}	0.5	G035.20−01.73	CCS	45	8.5×10^{12}	2.0		
C ¹⁸ O		85	4.3×10^{17}	0.		CH ₃ OH	85	1.0×10^{15}	1.5		
HNCO		45	2.5×10^{14}	0.		t-HCOOH	85	1.0×10^{14}	2.0		
C ¹⁵ N		45	8.5×10^{13}	0.		¹³ CN	85	1.2×10^{14}	2.0		
¹³ CO		85	9.2×10^{18}	0.		HC ₃ N	85	1.5×10^{14}	2.0		
CH ₃ CN	45	7.5×10^{14}	0.	SO		45	1.0×10^{15}	2.0			
CH ₃ OCHO	45	3.4×10^{14}	-0.5	OCS		45	4.0×10^{14}	2.0			
CH ₃ OCH ₃	45	1.0×10^{15}	1.0	C ¹⁸ O		85	1.1×10^{17}	2.0			
C ¹⁷ O	45	5.5×10^{16}	0.	HNCO		45	4.5×10^{13}	2.0			
CN	85	3.0×10^{16}	0.	C ¹⁵ N		45	4.0×10^{13}	2.0			
G009.62+00.19	NH ₂ CHO	45	7.0×10^{13}	1.0		¹³ CO	85	1.7×10^{18}	2.0		
	CCS	45	2.5×10^{13}	1.5		CH ₃ CN	45	4.1×10^{13}	2.0		
	HC ₅ N	45	2.0×10^{13}	1.5		CH ₃ CHO	45	1.0×10^{14}	2.0		
	C ₂ H ₅ OH	45	4.1×10^{14}	2.0		C ¹⁷ O	45	2.0×10^{16}	2.0		
	³⁴ S ₂ O	45	1.1×10^{14}	3.0		CN	45	3.0×10^{15}	1.0		
	CH ₃ OCH ₃	45	1.0×10^{15}	1.0	G037.43+01.51	CCS	45	1.7×10^{13}	3.0		
	OC ³⁴ S	45	2.3×10^{14}	2.0		HC ₅ N	45	1.2×10^{13}	3.5		
	CH ₃ OH	85	1.2×10^{16}	2.5		³⁴ S ₂ O	45	3.3×10^{13}	2.0		
	C ₂ H ₅ CN	45	7.3×10^{13}	3.0		CH ₃ OH	85	4.0×10^{15}	2.5		
	¹³ CH ₃ CN	45	5.5×10^{12}	2.0		CH ₃ OCHO	45	4.7×10^{14}	3.5		
	CH ₃ OCHO	45	1.3×10^{15}	2.0		SO ₂	85	4.5×10^{14}	3.0		
	t-HCOOH	45	6.7×10^{13}	1.5		t-HCOOH	85	1.5×10^{14}	3.0		
	¹³ CN	45	1.2×10^{14}	2.3		¹³ CN	85	1.0×10^{14}	2.5		
	HC ₃ N	85	9.2×10^{14}	2.0		HC ₃ N	85	1.7×10^{14}	3.0		
	SO	45	2.0×10^{15}	2.5		SO	45	1.3×10^{15}	3.0		
	HC ₃ N, $\nu_7=1$	85	6.5×10^{14}	1.0		OCS	45	4.7×10^{14}	3.0		
	OCS	45	2.7×10^{15}	2.5		HNCO	45	7.0×10^{13}	2.5		
	HNCO	45	1.2×10^{14}	2.0		C ¹⁸ O	85	1.9×10^{17}	3.0		
	C ¹⁸ O	85	4.3×10^{17}	2.0		C ¹⁵ N	45	1.0×10^{13}	2.5		
	C ¹⁵ N	45	1.5×10^{12}	2.5		¹³ CO	85	4.4×10^{18}	3.0		
	¹³ CO	85	8.5×10^{18}	2.5	CH ₃ CN	45	5.0×10^{13}	3.0			
	CH ₃ CN	45	2.0×10^{14}	2.0	CH ₃ OCH ₃	45	1.0×10^{15}	3.0			
	C ₂ H ₃ CN	45	1.1×10^{13}	2.5	CH ₃ CHO	45	1.3×10^{14}	3.0			
	CH ₃ CHO	45	1.4×10^{14}	2.0	C ¹⁷ O	45	2.6×10^{16}	3.0			
	C ¹⁷ O	45	7.0×10^{13}	1.5	CN	85	1.0×10^{15}	3.0			
CN	85	1.0×10^{16}	2.2								

Note. This is only a subset of the whole table, which is available in the supplementary material.

3 Results

3.1 Detections of molecular species

Molecules identified in each source are summarized in the second, third and fourth columns of Table 3. Excluding isotopologues, 27 compounds have been identified in

the 50 target massive star-forming regions, of which 16 species contain six or more atoms. The identified species cover 10 oxygen-bearing molecules, 5 sulfur-bearing molecules, 10 nitrogen-bearing molecules, 1 silicon-bearing molecule, and 1 ion. Particularly, SO, CN, HC₃N, and CH₃OH are detected in all sources, while CH₃CN

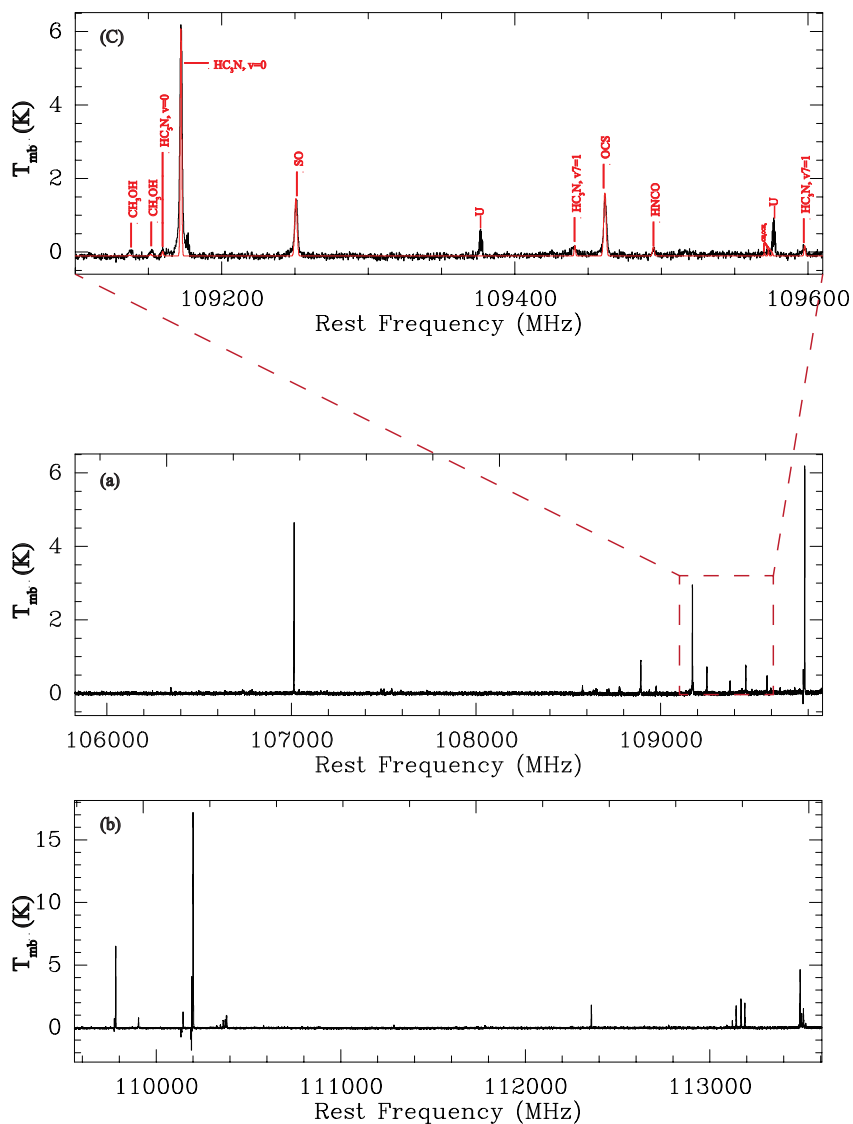


Fig. 1. (a) and (b): The observed lines that have subtracted baselines in G009.62+00.19. (c) Zoomed-in view of the modeling synthetic spectrum of the observed lines. The red solid line are the modeling synthetic spectrum.

is detected in all sources except for G168.06+00.82. On the other hand, some molecules were detected in most of sources, such as OCS (48 sources), HNCN (43 sources), CH₃CHO (42 sources), while some molecules were detected only in few sources, such as CH₃SH in G010.62–00.38, G012.80–00.20 and G049.48–00.36, CH₃COOH in G010.47+00.02, G049.48–00.36, and G049.48–00.38. Molecules chemically related with each other are discussed in Section 4.2. The only detected ion, HOCO⁺, is detailed in Section 4.3.

Lines of the detected molecules, above 3σ level in each source, are listed in Table 4, which include species, transitions, rest frequencies, upper level energy (E_u), line strength (i.e. dipole-weighted transition dipole matrix elements, μ^2S), peak intensity (T_{mb}), centroid velocity

(V_{LSR}), FWHM (ΔV), and integrated intensity ($\int T_{mb} dv$). Lines in different vibrational states, and with high E_u were also identified. For example, lines of HC₃N in $v_4=1$, $v_6=1$, $v_7=1$, $v_7=2$, $v_5=1/v_7=3$, and $v_6=v_7=1$, as well as CH₃CN in $v_8=1$, and C₂H₅CN with $v_{12}=1-A$, $v_{20}=1-A$ vibrational states with high E_u have been observed.

3.2 Radio recombination lines

Six radio recombination lines (RRLs) of hydrogen and three RRLs of helium were detected in this work, which are listed in the column (5) of Table 3. H (39) α is the strongest among the identified RRLs, detected in 20 sources. The He (39) α was detected in 7 sources, while He (48) β and He (55) γ were separately detected in G012.80–00.20 and

G209.00–19.38. Line parameters for the detections of H (39) α and He (39) α in the different sources are listed in Table 5.

3.3 Notes for individual sources

The detected molecules in G000.67–00.03 (Sgr B2), G010.47+00.02, G049.48–00.36, and G049.48–00.38 cover more than 98% of the identified species. The four sources are rich in 18, 25, 21, and 23 molecular species, respectively. On the other hand, some molecules were only detected in one or two of the four sources. For example, HCOCN and CH₃OCH₂OH were only detected in G010.47+00.02, while aGg'–(CH₂OH)₂ was detected in G010.47+00.02 and G049.48–00.38. The RRLs in G012.80–00.20 and G015.03–00.67 include all kinds of RRLs observed in this work.

3.4 Unidentified lines

The observed frequencies for the unidentified lines are listed in Table 6. The JPL and CDMS databases cannot provide any plausible carrier for these unidentified features, the line width of which ranges from 1.1 to 19.0 km/s. These unidentified lines with different widths for the same source are credible. The widths of unidentified lines are within the width range of those detected lines. For example, line widths of the detected lines and unidentified lines in G009.62+00.19 are from 0.5 to 19.1 km/s, and from 1.5 to 5.2 km/s, respectively. Only three of our target sources, G005.88–00.39, G031.28+00.06, and G111.54+00.77, have no unidentified features above 3σ level. In 33 sources, there are four or less than four lines above 3σ level left for identification. G049.48–00.38 (W 51M) has the largest number of unidentified features (40 in total), which deserves more attention for search of new interstellar molecules. Table 6 can be taken as a reference for follow-up in future works. Among these unidentified lines, H₂CCN and DCOOH might be the carriers, of which only one transition matches with the laboratory spectroscopic data in G005.88–00.39 and G009.62+00.19, respectively.

4 Discussion

4.1 Column Densities and Line Widths of the Detected Lines

To further elucidate the underlying similarities and correlations among various molecules, the Pearson's coefficient ($r_{Pearson}$) was employed to separately compare column densities (column (4) in Table 2) and line widths (FWHMs, column (8) in Table 4) of the detected lines, as derived from

the line-fitting procedure detailed in Section 2.2. Figure 2 visualizes this comparative analysis of line widths and column densities. The strong positive correlations ($r_{Pearson} > 0.80$) observed in both column densities and line widths provide further validation that SO, CCS, OCS, and SO₂, are chemically linked with each other, as discussed in Section 4.2.1. Using a similar approach, Fontani et al. (2023) reported poor correlations among the FWHMs of CCS, SO₂, and OCS across different evolutionary stages of 15 high-mass star-forming cores. These correlations could potentially become more robust if analyzed with identical data points align with that of this work. Furthermore, the strong correlations identified in this work suggest that these molecules, along with other chemically related species outlined in Sections 4.2.2 – 4.2.6, likely originate from similar gaseous environments within star-forming regions (Coletta et al. 2020).

4.2 Related Molecules in Chemistry

One way to investigate possible formation pathways of molecules is through statistically analyzing abundances of related molecules (Pilling et al. 2011; Peng et al. 2022). The related molecules, particularly complex organic molecules (COMs), are of considerable interest for studying the astro-chemical evolution where they reside (Herbst & van Dishoeck 2009), because COMs have the potential to form prebiotic molecules such as amino acids, sugars, and nucleobases (Gorai et al. 2020). Following the convention of Herbst & van Dishoeck (2009), a COM is defined as a molecule containing six or more atoms and 16 species of COMs have been detected in this work. The detection rates of the related molecules are listed in Table 7, which is convenient to study the potential formation routes of molecules and the physical properties, such as temperature and mass, of the environments where they reside.

4.2.1 SO, CCS, OCS, and SO₂

SO, CCS, OCS, and SO₂ are usually used to trace dense gas (Benson et al. 1998; Holdship et al. 2019; Xie et al. 2021), and may be chemically correlated with each other (Herpin et al. 2009; Li et al. 2015; Vidal & Wakelam 2018). For example, Vastel et al. (2018) focused on 21 sulfur-bearing species, including SO, CCS, OCS, and SO₂, to investigate sulfur chemistry in the L1544 prestellar core. Additionally, Fontani et al. (2023) modeled the chemistry of sulfur during the evolution of high-mass star-forming cores according to the detected lines of SO, SO⁺, NS, C³⁴S, ¹³CS, SO₂, CCS, H₂S, HCS⁺, OCS, H₂CS, and CCCS. In this work, the detection-rate of SO, CCS, OCS, and SO₂ are 100% (50), 92% (46), 96% (48), and 42% (21), respec-

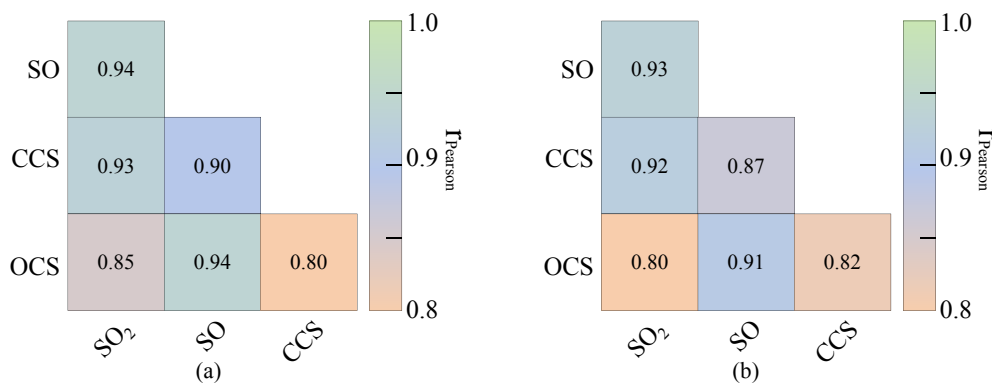


Fig. 2. Correlation matrix displaying the Pearson coefficients for (a) line widths and (b) column densities of the detected SO, CCS, OCS, and SO₂ in our sample.

tively, which are summarized in Table 8. All these four species were simultaneously detected in 20 sources being good candidates to study the sulfur chemistry.

4.2.2 CH₃OH, CH₃OCH₃, CH₃OCHO, CH₃CHO, C₂H₅OH, and CH₃COCH₃

CH₃OH, a key species in the formation of COMs, was exhaustively studied experimentally and found to be abundant and widespread in the ISM (Qin et al. 2022). CH₃OCH₃, CH₃OCHO, CH₃CHO, and C₂H₅OH are related with CH₃OH in chemistry (Lefloch et al. 2017; Singh et al. 2019; Chen et al. 2023). Their detection rates are 70% (35), 64% (32), 86% (43), and 24% (12), respectively, the detailed detection of which is given in Table 9. Our sample would be appreciated for statistically analyzing the relations among CH₃OCH₃, CH₃OCHO, and CH₃CHO.

CH₃COCH₃ is the simplest and smallest ketone, which was firstly detected in Sgr B2 by Combes et al. (1987) and later confirmed by Snyder et al. (2002). The distribution of CH₃COCH₃ is clearly different from those of typical oxygen-bearing molecules (CH₃OH, CH₃OCHO) in Orion KL (Friedel & Snyder 2008; Peng et al. 2013). The differences between CH₃COCH₃ and other large oxygen-bearing molecules make CH₃COCH₃ an excellent tool for testing different chemical models of complex molecules, i.e., in the gas phase by pure cosmic ray induced ion-molecule chemistry, on the surface of grains, or both. The formation of CH₃COCH₃ in space is still unclear. CH₃COCH₃ was only detected in 4 of our target sources (~10%), as shown in Table 9. High resolution spectral line surveys of large sample are needed to tackle the issue systematically.

4.2.3 HCOOH and CH₃COOH

HCOOH, the simplest carboxylic acid, together with its descendant CH₃COOH (Pilling et al. 2011), are possible precursors of prebiotic species (Fedoseev et al. 2015).

They have been extensively detected in the ISM (Schutte et al. 1999), comets (Bennett & Kaiser 2007) and meteorites (Bisschop et al. 2007). The detection-rate of HCOOH is 72% (36), while CH₃COOH was only detected in G010.47+00.02, G049.48–00.36, and G049.48–00.38, as summarized in Table 10.

4.2.4 HNCO and NH₂CHO

Both HNCO and NH₂CHO are potential prebiotic molecules that contain a peptide bond [–(H)N–C(O)–], which is the link of amino acids, and consequently form proteins. HNCO is the simplest molecule containing four of the six biogenic elements: carbon, hydrogen, oxygen, nitrogen, phosphorus, and sulfur that are present in all living beings, which has been identified in 43 out of our 50 target sources (~86%). NH₂CHO, one of the simplest organic amide, has been suggested to be crucial in the synthesis of metabolic and genetic molecules, the chemical basis of life (Saladino et al. 2012), and its detection rate is 50% (~25 sources). The summary of detected HNCO and NH₂CHO is listed in Table 11. Gorai et al. (2020) studied three nitrogen-bearing molecules (HNCO, NH₂CHO, and CH₃NCO) containing peptide-like bonds in G10.47+0.03 and found that HNCO, NH₂CHO, and CH₃NCO are chemically linked with each other. The chemical links between HNCO and NH₂CHO were confirmed by Taniguchi et al. (2023). Therefore, our sample can be used to systematically study the link between HNCO and NH₂CHO, which would shed a light on the evolution of amino acids in the ISM.

4.2.5 HC₃N and HC₅N

HC₃N, and HC₅N are two of carbon-chain species that are prone to be depleted onto dust grains when the gas is cold, and destroyed by UV radiations (Sakai & Yamamoto 2013), the detected of which in our sample is presented in Table 12. HC₃N and HC₅N were first detected in Sgr

B2 (Turner 1971; Broten et al. 1976), and have been found to be widespread in the Milky Way ISM (Crovisier et al. 2004; Fontani et al. 2017; Taniguchi et al. 2019; Wang et al. 2022). Their detection rates in our sample are 100% (50) and 58% (29), respectively.

4.2.6 CN, CH₃CN, C₂H₃CN, and C₂H₅CN

CN, the first observed nitrogen-bearing species in the ISM (McKellar 1940), can be produced from HCN via photodissociation and from reactions involving C⁺ and C (Boger & Sternberg 2005). CN can be thus taken as a probe of dense gas exposed to strong ultraviolet (UV) radiation in photon-dominated regions (PDRs). Formation of CN at high column densities can be driven by enhanced cosmic ray ionization rates (Boger & Sternberg 2005) or by X-rays near an active galactic nucleus (AGN) as shown by models of X-ray-dominated regions (Meijerink et al. 2007; Wolfire et al. 2022). CN was detected in all sources of our sample, which combined with known PDRs deserves further study of dense gas properties.

CH₃CN, C₂H₃CN, and C₂H₅CN were found to be related with CN (Zeng et al. 2018; Ribeiro et al. 2020). CH₃CN is present in all sources except for G168.06+00.82, while C₂H₃CN and C₂H₅CN were observed in 16 (~32%) and 20 (~40%) sources of our sample, respectively. The relation between C₂H₃CN and C₂H₅CN can be studied with the target sources hosting them. We summarized the detected CN, CH₃CN, C₂H₃CN, and C₂H₅CN in Table 13.

4.3 The detected ion HOCO⁺

CO₂, lack of a permanent dipole moment, is an important reservoir of carbon and oxygen, and one of the major constituents of the icy mantles of dust grains. The protonated form of CO₂, HOCO⁺, is an interesting alternative to track the gas phase CO₂ in the millimeter/sub-millimeter regime. Fontani et al. (2018) first represented the statistical study of protonated carbon dioxide in 11 massive star-forming regions, and found that the ion-radical reaction $HCO^+ + OH \rightarrow HOCO^+ + H$ plays a more important role than a direct protonation of CO₂ in the gas-phase formation route of HOCO⁺. Particularly, two transitions of HOCO⁺, $4_{0,4} - 3_{0,3}$ (85531.497 MHz) and $5_{0,5} - 4_{0,4}$ (106913.545 MHz), have been observed in IRAS 16293 – 2422 to study the chemistry of CO₂ ices according to Majumdar et al. (2018). In our work, the transition $5_{0,5} - 4_{0,4}$ also has been detected in G010.47+00.02 and G081.87+00.78, while it is marginally detected in G049.48–00.38, G133.94+01.06, and G183.72+03.66, graphically shown in Figure 3. Additionally, the transition $5_{1,4} - 4_{1,3}$ (107315.356 MHz) is weaker than $5_{0,5} -$

$4_{0,4}$, and has been marginally detected in the five sources (Figure 3). Our target sources, where HOCO⁺ was detected, enlarge the sample size to study the formation of HOCO⁺, and therefore might advance the understanding of its interstellar chemistry.

4.4 Lines in vibrational state and with high E_u

Molecular complexity in the ISM is not only manifest in increasingly larger molecules, but also in excited vibrational states of abundant molecules. The vibrational transitions generally have high upper level energy (E_u) compared with the ground state transitions, which emit radiation from the centimeter to sub-millimeter wavelength, unaffected by the dust extinction, making them powerful tools to probe the energetic processes taking place in the innermost regions of heavily obscured galactic nuclei (Rico-Villas et al. 2021). On the other hand, combined with ground state lines, vibrational lines can be used to investigate the physical dynamic parameters, such as the gas distribution, velocity structure (Qin et al. 2015), and the astro-chemical evolution of the sources where they reside. Vibrationally excited lines HC₃N $v_7=1$ were observed in 24 of our target sources, while HC₃N $v_4=1$, $v_5=1/v_7=3$, $v_6=1$, $v_6=7=1$, and $v_7=2$, C₂H₅CN $v_{12}=1-A$ and $v_{20}=1-A$ were only detected in G10.47+00.02. CH₃CN $v_8=1$ and SO₂ $v_2=1$ were respectively identified in 3 (G10.47+00.02, G049.48–00.36, and G049.48–00.38) and 4 (G10.47+00.02, G043.16+00.01, G049.48–00.36, and G049.48–00.38) target sources, as summarized in Table 14. Therefore, G10.47+00.02, G043.16+00.01, G049.48–00.36, and G049.48–00.38 deserve to be systematically studied their astro-chemical evolution and physical dynamics with high sensitivity maps.

5 Summary

We have performed high-sensitivity broadband spectroscopic observations toward 50 massive star-forming regions with IRAM 30-m millimeter telescope. Weeds was used to identify molecules in each star-forming region. The related parameters, such as peak temperature, integrated intensity, and line width of the identified molecular lines were obtained. Even though no new molecule is discovered, the results provide a valuable dataset for further studies on the astro-chemical evolution of molecules in massive star-forming cores. Our main results are as follows:

1. There are 27 identified species, of which 16 are complex organic molecules.
2. Some chemically related molecules with high detection rate (> 60%), such as CH₃OCH₃ (~64%), CH₃OCHO

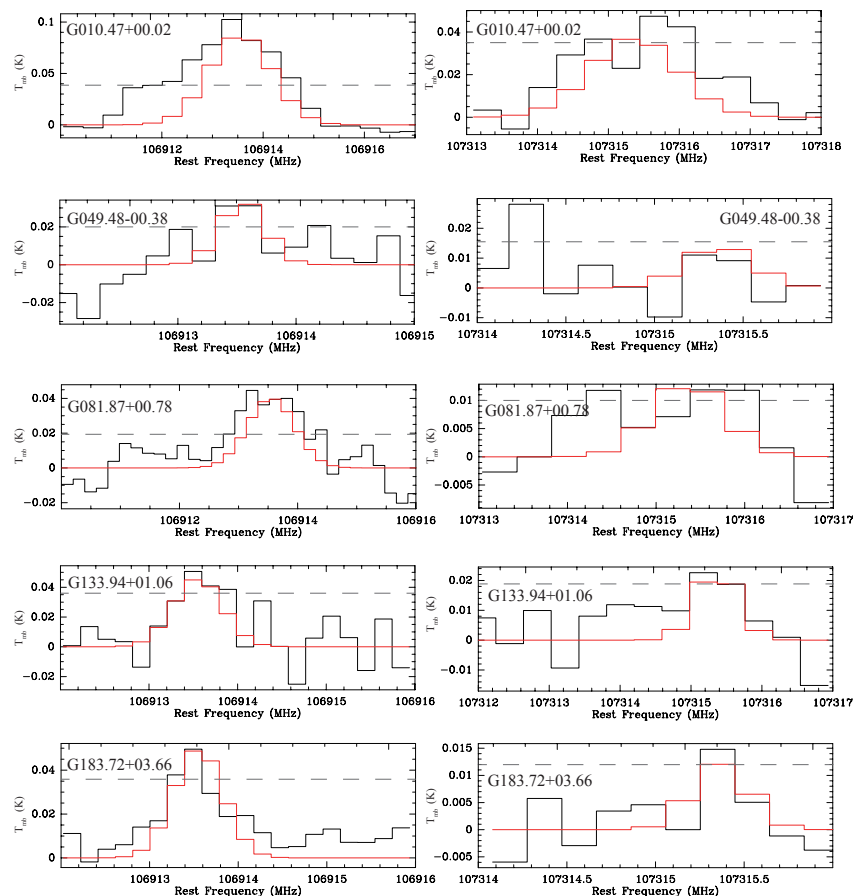


Fig. 3. The detected two transitions of HOCO^+ in 5 target sources. Black lines, red lines, and dash lines are observed lines, modeling synthetic spectrum, and 3σ level, respectively.

($\sim 64\%$), and CH_3CHO ($\sim 84\%$), deserve to be statistically investigated their correlations and possible evolution pathways.

3. The line widths of the chemically related molecules exhibit minimal fluctuations, suggesting they likely originate from similar gases in star-forming regions.
4. The transition of HOCO^+ , $5_{0,5} - 4_{0,4}$ (106913.545 MHz), is detected in G010.47+00.02 and G081.87+00.78, while it is marginally detected in G049.48-00.38, G133.94+01.06, and G183.72+03.66.

Supplementary data

The completed tables 2 and 4 are available in the supplementary material.

Acknowledgments

This work is supported by the National Natural Science Foundation of China (grant No. 12103010 and U1931104), Project funded by China Postdoctoral Science Foundation (Grant No. 2022M710016), Fundamental Research Funds for the Central Universities (Grant No. 2020CDJXZ002),

Chongqing Municipal Natural Science Foundation General Program (Grant No. cstc2021jcyj-msxmX0867), and Chongqing Talents: Exceptional Young Talents Project (Grant No. cstc2021ycjh-bgzxm0027). This study is based on observations carried out under project numbers 012-16 and 023-17 with the IRAM 30-m telescope. IRAM 30-m is supported by INSU/CNRS (France), MPG (Germany) and IGN (Spain).

Data Availability

The original data observed with IRAM 30-m can be accessed by IRAM archive system ². If anyone is interested in the reduced data presented in this paper, please contact Junzhi Wang at junzhiwang@gxu.edu.cn.

References

- Belloche, A., Garrod, R. T., Müller, H. S. P., et al. 2019, *A&A*, 628, A10.
 Belloche, A., Meshcheryakov, A. A., Garrod, R. T., et al. 2017, *A&A*, 601, A49.
 Belloche, A., Müller, H. S. P., Menten, K. M., et al. 2013, *A&A*,

² <https://www.iram-institute.org/EN/content-page-386-7-386-0-0-0.html>

- 559, A47.
- Bennett, C. J. & Kaiser, R. I. 2007, *ApJ*, 660, 1289.
- Benson, P. J., Caselli, P., & Myers, P. C. 1998, *ApJ*, 506, 743.
- Bernal, J. J., Koelemay, L. A., & Ziurys, L. M. 2021, *ApJ*, 906, 55.
- Bisschop, S. E., Fuchs, G. W., Boogert, A. C. A., et al. 2007, *A&A*, 470, 749.
- Boger, G. I. & Sternberg, A. 2005, *ApJ*, 632, 302.
- Bonfand, M., Belloche, A., Garrod, R. T., et al. 2019, *A&A*, 628, A27.
- Brotten, N. W., MacLeod, J. M., Oka, T., et al. 1976, *ApJL*, 209, L143.
- Ceccarelli, C., Codella, C., Balucani, N., et al. 2023, *Protostars and Planets VII*, 534, 379
- Cernicharo J., Agúndez M., Cabezas C., Fuentetaja R., Tercero B., Marcelino N., Endo Y., et al., 2022, *A&A*, 657, L16.
- Chen, Y., van Gelder, M. L., Nazari, P., et al. 2023, *A&A*, 678, A137.
- Coletta, A., Fontani, F., Rivilla, V. M., et al. 2020, *A&A*, 641, A54.
- Combes, F., Gerin, M., Wootten, A., et al. 1987, *A&A*, 180, L13.
- Crovisier, J., Bockelée-Morvan, D., Colom, P., et al. 2004, *A&A*, 418, 1141.
- Endres, C. P., Schlemmer, S., Schilke, P., et al. 2016, *Journal of Molecular Spectroscopy*, 327, 95.
- Fedoseev, G., Ioppolo, S., Zhao, D., et al. 2015, *MNRAS*, 446, 439.
- Feng, S., Beuther, H., Henning, T., et al. 2015, *A&A*, 581, A71.
- Fontani, F., Roueff, E., Colzi, L., et al. 2023, *A&A*, 680, A58.
- Fontani F., Vagnoli A., Padovani M., Colzi L., Caselli P., Rivilla V. M., 2018, *MNRAS*, 481, 79.
- Fontani, F., Ceccarelli, C., Favre, C., et al. 2017, *A&A*, 605, A57.
- Fontani, F., Pascucci, I., Caselli, P., et al. 2007, *A&A*, 470, 639.
- Foster, J. B., Jackson, J. M., Barnes, P. J., et al. 2011, *ApJS*, 197, 25
- Frayer, D. T., Maddalena, R. J., Meijer, M., et al. 2015, *AJ*, 149, 162.
- Friedel, D. N. & Snyder, L. E. 2008, *ApJ*, 672, 962.
- Gibb, E., Nummelin, A., Irvine, W. M., et al. 2000, *ApJ*, 545, 309.
- Goddi, C., Greenhill, L. J., Humphreys, E. M. L., et al. 2009, *ApJ*, 691, 1254.
- Gorai, P., Bhat, B., Sil, M., et al. 2020, *ApJ*, 895, 86.
- Corby, J. F., McGuire, B. A., Herbst, E., et al. 2018, *A&A*, 610, A10.
- Herbst E., van Dishoeck E. F., 2009, *ARA&A*, 47, 427.
- Hernández-Hernández, V., Kurtz, S., Kalenskii, S., et al. 2019, *AJ*, 158, 18.
- Herpin, F., Marseille, M., Wakelam, V., et al. 2009, *A&A*, 504, 853.
- Holdship, J., Jimenez-Serra, I., Viti, S., et al. 2019, *ApJ*, 878, 64.
- Hollis, J. M., Jewell, P. R., Lovas, F. J., et al. 2004, *ApJL*, 610, L21.
- Jones, P. A., Burton, M. G., Cunningham, M. R., et al. 2008, *MNRAS*, 386, 117.
- Jones, P. A., Burton, M. G., Cunningham, M. R., et al. 2012, *MNRAS*, 419, 2961.
- Jørgensen J. K., Belloche A., Garrod R. T., 2020, *ARA&A*, 58, 727.
- Kolesníková, L., Belloche, A., Koucký, J., et al. 2022, *A&A*, 659, A111.
- Lee, C. W. & Cho, S.-H. 2002, *Journal of Korean Astronomical Society*, 35, 187.
- Lefloch, B., Ceccarelli, C., Codella, C., et al. 2017, *MNRAS*, 469, L73.
- Li, J., Wang, J., Zhu, Q., et al. 2015, *ApJ*, 802, 40.
- Li, J., Wang, J., Qiao, H., et al. 2020, *MNRAS*, 492, 556.
- Li, J., Wang, J., Lu, X., et al. 2021, *ApJ*, 919, 4.
- Li, Y., Wang, J., Li, J., et al. 2022, *MNRAS*, 512, 4934.
- Liu, X., Liu, T., Shen, Z., et al. 2022, *ApJS*, 263, 13.
- Majumdar L., Gratier P., Wakelam V., Caux E., Willacy K., Ressler M. E., 2018, *MNRAS*, 477, 525.
- Maret, S., Hily-Blant, P., Pety, J., Bardeau, S., & Reynier, E. 2011, *A&A*, 526, A47.
- Margulès L., Remijan A., Belloche A., Motiyenko R. A., McGuire B. A., Xue C., Müller H. S. P., et al., 2022, *A&A*, 663, A132.
- Massalkhi, S., Agúndez, M., & Cernicharo, J. 2019, *A&A*, 628, A62.
- McKellar, A. 1940, *PASP*, 52, 187.
- Meijerink, R., Spaans, M., & Israel, F. P. 2007, *A&A*, 461, 793.
- Motte, F., Bontemps, S., & Louvet, F. 2018, *ARA&A*, 56, 41.
- Müller, H. S. P., Schlöder, F., Stutzki, J., et al. 2005, *Journal of Molecular Structure*, 742, 215.
- Ospina-Zamudio, J., Lefloch, B., Ceccarelli, C., et al. 2018, *A&A*, 618, A145.
- Pardo J. R., Cernicharo J., Tercero B., Cabezas C., Bermúdez C., Agúndez M., Gallego J. D., et al. 2022, *A&A*, 658, A39.
- Peng, Y., Liu, T., Qin, S.-L., et al. 2022, *MNRAS*, 512, 4419.
- Peng, T.-C., Despois, D., Brouillet, N., et al. 2013, *A&A*, 554, A78.
- Pickett, H. M., Poynter, R. L., Cohen, E. A., et al. 1998, *J. Quant. Spectrosc. Radiat. Transfer*, 60, 883.
- Pilling, S., Baptista, L., Boechat-Roberty, H. M., et al. 2011, *Astrobiology*, 11, 883.
- Podio, L., Codella, C., Lefloch, B., et al. 2017, *MNRAS*, 470, L16.
- Qin, S.-L., Liu, T., Liu, X., et al. 2022, *MNRAS*, 511, 3463.
- Qin, S.-L., Schilke, P., Wu, J., et al. 2015, *ApJ*, 803, 39.
- Reid, M. J., Menten, K. M., M., Brunthaler, A., et al. 2014, *ApJ*, 783, 130.
- Remijan, A., Snyder, L. E., Friedel, D. N., et al. 2003, *ApJ*, 590, 314.
- Ribeiro, F. de A., Almeida, G. C., Wolff, W., et al. 2020, *MNRAS*, 492, 2140.
- Rico-Villas, F., Martín-Pintado, J., González-Alfonso, E., et al. 2021, *MNRAS*, 502, 3021.
- Sakai, N. & Yamamoto, S. 2013, *Chemical Reviews*, 113, 8981.
- Saladino, R., Botta, G., Pino, S., et al. 2012, *Chem Soc Rev*, 41, 5526.
- Sanz-Novo, M., Belloche, A., Alonso, J. L., et al. 2020, *A&A*,

- 639, A135.
- Schilke, P., Groesbeck, T. D., Blake, G. A., et al. 1997, *ApJS*, 108, 301.
- Schilke, P., Comito, C., Thorwirth, S., et al. 2006, *A&A*, 454, L41.
- Schutte, W. A., Boogert, A. C. A., Tielens, A. G. G. M., et al. 1999, *A&A*, 343, 966.
- Singh, S. C., Twagirayezu, S., Muckle, M., et al. 2019, 74th International Symposium on Molecular Spectroscopy.
- Snyder, L. E., Lovas, F. J., Mehringer, D. M., et al. 2002, *ApJ*, 578, 245.
- Suzuki, T., Ohishi, M., Saito, M., et al. 2018, *ApJS*, 237, 3.
- Sutton, E. C., Peng, R., Danchi, W. C., et al. 1995, *ApJS*, 97, 455.
- Taniguchi, K., Sanhueza, P., Olguin, F. A., et al. 2023, *ApJ*, 950, 57.
- Taniguchi, K., Herbst, E., Caselli, P., et al. 2019, *ApJ*, 881, 57.
- Tercero, B., Vincent, L., Cernicharo, J., et al. 2011, *A&A*, 528, A26.
- Turner, B. E. 1971, *ApJL*, 163, L35.
- van der Tak, F. F. S., van Dishoeck, E. F., & Caselli, P. 2000, *A&A*, 361, 327.
- van der Walt, S. J., Kristensen, L. E., Jørgensen, J. K., et al. 2021, *A&A*, 655, A86.
- Vastel, C., Quénard, D., Le Gal, R., et al. 2018, *MNRAS*, 478, 5514.
- Vasyunina, T., Vasyunin, A. I., Herbst, E., et al. 2014, *ApJ*, 780, 85.
- Vidal, T. H. G. & Wakelam, V. 2018, *MNRAS*, 474, 5575.
- Wang, Y. X., Zhang, J. S., Yan, Y. T., et al. 2022, *A&A*, 663, A177.
- Widicus Weaver, S. L., Laas, J. C., Zou, L., et al. 2017, *ApJS*, 232, 3.
- Wilkins, O. H., Carroll, P. B., & Blake, G. A. 2022, *ApJ*, 924, 4.
- White, G. J., Araki, M., Greaves, J. S., et al. 2003, *A&A*, 407, 589.
- Wolfire, M. G., Vallini, L., & Chevance, M. 2022, *ARA&A*, 60, 247.
- Xie, J., Fuller, G. A., Li, D., et al. 2021, *Science China Physics, Mechanics, and Astronomy*, 64, 279511.
- Zeng, S., Jiménez-Serra, I., Rivilla, V. M., et al. 2018, *MNRAS*, 478, 2962.
- Ziurys, L. M. & McGonagle, D. 1993, *ApJS*, 89, 155.

Table 3. Detected molecules and radio recombination line in sources.

Source (1)	< 6 Atoms (2)	≥ 6 Atoms (3)	Isotopic molecules (4)	Radio recombination line (5)	N* (6)
G000.67-00.03	SO, SiS, CCS, OCS, SO ₂ , HNC, HC ₃ N, t-HCOOH	NH ₂ CHO, CH ₃ OH, HC ₅ N, CH ₃ CN, C ₂ H ₃ CN, CH ₃ OCHO, C ₂ H ₅ CN, C ₂ H ₅ OH, CH ₃ CHO, CH ₃ OCH ₃	³⁴ SO, OC ³⁴ S, CH ₃ C ¹⁵ N, ¹³ CH ₃ CN, C ¹⁸ O, ¹³ CO, CH ₃ ¹³ CN, C ¹⁷ O	H (39) α, H (48) β	26
G005.88-00.39	SO, CN, CCS, OCS, SO ₂ , HNC, HC ₃ N	CH ₃ OH, CH ₃ CN, HC ₅ N, C ₂ H ₃ CN, CH ₃ OCHO, CH ₃ C ₃ N, CH ₃ OCH ₃	¹³ CN, C ¹⁸ O, C ¹⁵ N, ¹³ CO, C ¹⁷ O	H (39) α, H (48) β, H (55) γ	19
G009.62+00.19	SO, CN, CCS, OCS, HNC, t-HCOOH, HC ₃ N	NH ₂ CHO, CH ₃ OH, CH ₃ CN, HC ₅ N, C ₂ H ₃ CN, CH ₃ CHO, C ₂ H ₅ OH, C ₂ H ₅ CN, CH ₃ OCHO, CH ₃ OCH ₃	³⁴ SO, OC ³⁴ S, ¹³ CH ₃ CN, ¹³ CN, C ¹⁸ O, C ¹⁵ N, ¹³ CO, C ¹⁷ O	H (39) α, He (39) α	25
G010.47+00.02	SO, SiS, CN, CCS, OCS, SO ₂ , HOCO ⁺ , HNC, HC ₃ N, HCOCN, t-HCOOH	NH ₂ CHO, CH ₃ OH, CH ₃ CN, HC ₅ N, C ₂ H ₃ CN, CH ₃ CHO, CH ₃ OCHO, CH ₃ COOH, C ₂ H ₅ OH, C ₂ H ₅ CN, CH ₃ OCH ₃ , CH ₃ COCH ₃ , CH ₃ OCH ₂ OH, CH ₃ C ₃ N, aGg ⁺ -(CH ₂ OH) ₂	¹³ CH ₃ CH ₂ CN, ³⁴ SO, C ₂ CH ₅ ¹³ CN, ¹³ CN, OC ³⁴ S, ¹³ CH ₃ CN, CH ₃ ¹³ CH ₂ CN, C ¹⁸ O, OC ³³ S, O ¹³ CS, CH ₃ ¹³ CN, ¹³ CO, ¹³ CH ₂ CHCN, C ¹⁷ O	non-detection	40
G010.62-00.38	SO, CN, SiS, CCS, OCS, SO ₂ , SO ₂ , HC ₃ N, t-HCOOH	NH ₂ CHO, CH ₃ OH, CH ₃ SH, CH ₃ CN, HC ₅ N, C ₂ H ₃ CN, CH ₃ CHO, CH ₃ OCHO, CH ₃ OCH ₃ , C ₂ H ₅ OH, C ₂ H ₅ CN	OC ³⁴ S, ¹³ CH ₃ CN, ¹³ C ¹⁷ O, ¹³ CN, C ¹⁸ O, C ¹⁵ N, ¹³ CO, C ¹⁷ O	H (39) α, He (39) α, H (55) γ, H (48) β, H (64) ε	27
G011.49-01.48	SO, CN, HC ₃ N	CH ₃ OH, CH ₃ CN	¹³ CN, C ¹⁸ O, ¹³ CO, C ¹⁷ O	non-detection	9
G011.91-00.61	SO, CN, CCS, OCS, HNC, HC ₃ N, t-HCOOH	NH ₂ CHO, CH ₃ OH, CH ₃ CN, HC ₅ N, C ₂ H ₃ CN, CH ₃ CHO, CH ₃ OCHO, CH ₃ OCH ₃	¹³ CN, C ¹⁸ O, C ¹⁵ N, ¹³ CO, C ¹⁷ O	non-detection	21
G012.80-00.20	SO, CN, CCS, OCS, HNC, t-HCOOH, HC ₃ N	NH ₂ CHO, CH ₃ OH, CH ₃ SH, CH ₃ CN, HC ₅ N, C ₂ H ₃ CN, CH ₃ CHO, CH ₃ C ₃ N, CH ₃ OCH ₃	¹³ C ¹⁷ O, ¹³ CN, C ¹⁸ O, ¹³ CO, C ¹⁷ O	H (39) α, He (39) α, H (65) ε, H (55) γ, H (60) δ, H (48) β, He (48) β, H (64) ε	22
G012.88+00.48	SO, CN, CCS, OCS, HC ₃ N, HNC, SO ₂ , t-HCOOH	NH ₂ CHO, CH ₃ OH, CH ₃ CN, HC ₅ N, C ₂ H ₃ CN, CH ₃ CHO, CH ₃ OCHO, C ₂ H ₅ OH, C ₂ H ₅ CN, CH ₃ OCH ₃	³⁴ SO, OC ³⁴ S, ¹³ CH ₃ CN, ¹³ C ¹⁷ O, ¹³ CN, C ¹⁸ O, C ¹⁵ N, ¹³ CO, C ¹⁷ O	non-detection	27
G012.90-00.24	SO, CN, OCS, HNC, HC ₃ N	CH ₃ OH, CH ₃ CN	C ¹⁸ O, ¹³ CO, C ¹⁷ O	non-detection	10
G012.90-00.26	SO, CN, OCS, SO ₂ , HNC, HC ₃ N	NH ₂ CHO, CH ₃ OH, CH ₃ CN, CH ₃ CHO, CH ₃ OCHO, C ₂ H ₅ CN, CH ₃ OCH ₃	³⁴ SO, OC ³⁴ S, ¹³ CN, C ¹⁸ O, ¹³ CO, C ¹⁷ O	non-detection	19
G014.33-00.64	SO, CN, CCS, OCS, HNC, HC ₃ N, t-HCOOH	NH ₂ CHO, CH ₃ OH, CH ₃ CN, CH ₃ CHO, CH ₃ OCHO, HC ₅ N, CH ₃ OCH ₃	OC ³⁴ S, ¹³ CN, C ¹⁸ O, C ¹⁵ N, ¹³ CO, C ¹⁷ O	non-detection	20
G015.03-00.67	SO, CN, OCS, CCS, HNC, HC ₃ N	CH ₃ OH, CH ₃ CN, HC ₅ N	¹³ CN, C ¹⁸ O, C ¹⁵ N, ¹³ CO, C ¹⁷ O	H (39) α, He (39) α, H (65) ε, H (55) γ, H (60) δ, H (48) β, H (64) ε	9
G016.58-00.05	SO, CN, OCS, CCS, HNC, HC ₃ N	CH ₃ OH, CH ₃ CN, CH ₃ CHO, CH ₃ OCHO, CH ₃ OCH ₃ , C ₂ H ₅ CN	OC ³⁴ S, O ¹³ CS, ¹³ C ¹⁷ O, ¹³ CN, C ¹⁸ O, ¹³ CO, C ¹⁷ O	non-detection	19
G023.00-00.41	SO, CN, OCS, CCS, HC ₃ N, HNC	NH ₂ CHO, CH ₃ OH, CH ₃ CN, HC ₅ N, C ₂ H ₃ CN, CH ₃ CHO, CH ₃ OCHO, C ₂ H ₅ CN, CH ₃ OCH ₃	¹³ CN, C ¹⁸ O, ¹³ CO, C ¹⁷ O	non-detection	19
G023.44-00.18	SO, CN, OCS, HNC, HC ₃ N, t-HCOOH	NH ₂ CHO, CH ₃ OH, CH ₃ CN, CH ₃ CHO, CH ₃ OCHO, CH ₃ OCH ₃	OC ³⁴ S, ¹³ C ¹⁷ O, ¹³ CN, C ¹⁸ O, ¹³ CO, C ¹⁷ O	H (39) α	19
G027.36-00.16	SO, CN, OCS, CCS, HNC, t-HCOOH, HC ₃ N	NH ₂ CHO, CH ₃ OH, CH ₃ CN, HC ₅ N, C ₂ H ₃ CN, CH ₃ CHO, CH ₃ OCHO, C ₂ H ₅ OH, C ₂ H ₅ CN, CH ₃ OCH ₃ , CH ₃ COCH ₃	OC ³⁴ S, ¹³ CH ₂ CN, ¹³ C ¹⁷ O, OC ³³ S, ¹³ CN, O ¹³ CS, C ¹⁸ O, ¹³ CO, CH ₃ ¹³ CN, C ¹⁷ O	H (39) α	28
G028.86+00.06	SO, CN, OCS, CCS, SO ₂ , HNC, t-HCOOH, HC ₃ N	NH ₂ CHO, CH ₃ OH, CH ₃ CN, CH ₃ CHO, C ₂ H ₅ CN, HC ₅ N, CH ₃ OCH ₃	¹³ C ¹⁷ O, ¹³ CN, C ¹⁸ O, ¹³ CO, C ¹⁷ O	non-detection	15
G029.95-00.01	SO, CN, OCS, CCS, HNC, t-HCOOH, HC ₃ N	NH ₂ CHO, CH ₃ OH, HC ₅ N, CH ₃ CN, C ₂ H ₃ CN, CH ₃ CHO, CH ₃ OCHO, C ₂ H ₅ CN, CH ₃ OCH ₃	OC ³⁴ S, ¹³ CN, C ¹⁸ O, ¹³ CO, C ¹⁷ O	H (39) α, H (55) γ, H (48) β	21
G031.28+00.06	SO, CN, OCS, CCS, HNC, HC ₃ N, t-HCOOH	NH ₂ CHO, CH ₃ OH, CH ₃ CN, CH ₃ CHO, CH ₃ OCHO, C ₂ H ₃ CN, CH ₃ OCH ₃	OC ³⁴ S, ¹³ CN, C ¹⁸ O, C ¹⁵ N, ¹³ CO, C ¹⁷ O	H (39) α	21
G031.58+00.07	SO, CN, OCS, CCS, HNC, HC ₃ N	CH ₃ OH, CH ₃ CN, HC ₅ N, C ₂ H ₃ CN, CH ₃ CHO, CH ₃ OCHO, CH ₃ OCH ₃	¹³ CN, C ¹⁸ O, ¹³ CO, C ¹⁷ O	non-detection	17
G032.04+00.05	SO, CN, OCS, CCS, HNC, HC ₃ N, t-HCOOH	NH ₂ CHO, CH ₃ OH, CH ₃ CN, HC ₅ N, CH ₃ CHO, CH ₃ OCHO, C ₂ H ₅ CN, CH ₃ OCH ₃	O ³⁴ S, OC ³⁴ S, ¹³ CH ₃ CN, ¹³ CN, C ¹⁸ O, ¹³ CO, C ¹⁷ O	non-detection	22
G034.39+00.22	SO, CN, SiS, OCS, CCS, HNC, HC ₃ N, t-HCOOH	NH ₂ CHO, CH ₃ OH, CH ₃ CN, CH ₃ CHO, CH ₃ OCHO, HC ₅ N, CH ₃ OCH ₃	¹³ CN, C ¹⁸ O, ¹³ CO, C ¹⁷ O	non-detection	19
G035.02+00.34	SO, CN, OCS, CCS, HNC, t-HCOOH, HC ₃ N	CH ₃ OH, CH ₃ CN, HC ₅ N, CH ₃ CHO	³⁴ SO, ¹³ CN, C ¹⁸ O, ¹³ CO, C ¹⁷ O	non-detection	16
G035.19-00.74	SO, CN, OCS, CCS, SO ₂ , HNC, HC ₃ N, t-HCOOH	NH ₂ CHO, CH ₃ OH, CH ₃ CN, CH ₃ CHO, CH ₃ OCHO, HC ₅ N, CH ₃ OCH ₃	³⁴ SO, OC ³⁴ S, ¹³ CN, C ¹⁸ O, C ¹⁵ N, ¹³ CO, C ¹⁷ O	non-detection	22

Table 3. (Continued)

Source (1)	< 6 Atoms (2)	≥ 6 Atoms (3)	Isotopic molecules (4)	Radio recombination line (5)	N* (6)
G035.20-01.73	SO, CN, OCS, CCS, HNCO, t-HCOOH, HC ₃ N	CH ₃ OH, CH ₃ CN, CH ₃ CHO	¹³ CN, C ¹⁸ O, C ¹⁵ N, ¹³ CO, C ¹⁷ O	H (39) α, H (55) γ, H (48) β	15
G037.43+01.51	SO, CN, OCS, CCS, SO ₂ , HNCO, t-HCOOH, HC ₃ N	CH ₃ OH, CH ₃ CN, HC ₅ N, CH ₃ CHO, CH ₃ OCHO, CH ₃ OCH ₃	³⁴ SO, ¹³ CN, C ¹⁸ O, C ¹⁵ N, ¹³ CO, C ¹⁷ O	non-detection	20
G043.16+00.01	SO, CN, OCS, CCS, SO ₂ , HNCO, HC ₃ N, t-HCOOH	CH ₃ OH, CH ₃ CN, CH ₃ CHO, CH ₃ OCHO, C ₂ H ₅ CN, CH ₃ OCH ₃	³⁴ SO, ³³ SO, ¹³ CN, C ¹⁸ O, ¹³ CO, C ¹⁷ O	H (39) α, He (39) α, H (65) ε, H (55) γ, H (48) β	20
G043.79-00.12	SO, CN, OCS, CCS, SO ₂ , HNCO, HC ₃ N, t-HCOOH	NH ₂ CHO, CH ₃ OH, CH ₃ CN, CH ₃ CHO, CH ₃ OCHO, C ₂ H ₅ CN, CH ₃ OCH ₃	OC ³⁴ S, ³⁴ SO, ¹³ CN, ¹³ C ¹⁷ O, C ¹⁸ O, C ¹⁵ N, ¹³ CO, C ¹⁷ O	H (39) α	23
G049.48-00.36	SO, CN, OCS, CCS, SO ₂ , t-HCOOH, HNCO, HC ₃ N	NH ₂ CHO, CH ₃ OH, CH ₃ SH, CH ₃ CN, HC ₅ N, C ₂ H ₅ CN, CH ₃ CHO, C ₂ H ₅ CN, CH ₃ OCHO, CH ₃ COOH, C ₂ H ₅ OH, CH ₃ OCH ₃ , CH ₃ COCH ₃	¹³ CH ₃ CN, ¹³ CN, ¹³ C ¹⁷ O, C ¹⁸ O, C ¹⁵ N, ¹³ CO, CH ₃ ¹³ CN, C ¹⁷ O	H (39) α, He (39) α, H (65) ε, H (48) β	29
G049.48-00.38	SO, CN, SiS, OCS, CCS, SO ₂ , HNCO, HOCO ⁺ , HC ₃ N, t-HCOOH	NH ₂ CHO, CH ₃ OH, CH ₃ CN, HC ₅ N, C ₂ H ₅ CN, CH ₃ CHO, C ₂ H ₅ CN, C ₂ H ₅ OH, CH ₃ OCHO, CH ₃ COOH, CH ₃ OCH ₃ , CH ₃ COCH ₃ , aGg ⁻ -(CH ₂ OH) ₂	OC ³⁴ S, ³⁴ SO, ¹³ CN, C ¹⁸ O, ¹³ CH ₃ CN, OC ³³ S, O ¹³ C ¹⁸ S, ¹³ CO, CH ₃ ¹³ CN, C ¹⁷ O	H (39) α, H (48) β	33
G059.78+00.06	SO, CN, OCS, CCS, HNCO, HC ₃ N, t-HCOOH	CH ₃ OH, CH ₃ CN, HC ₅ N, CH ₃ CHO	¹³ CN, C ¹⁸ O, C ¹⁵ N, ¹³ CO, C ¹⁷ O	non-detection	16
G069.54-00.97	SO, CN, OCS, CCS, SO ₂ , HNCO, HC ₃ N, t-HCOOH	CH ₃ OH, CH ₃ CN, HC ₅ N, CH ₃ CHO, CH ₃ OCHO, CH ₃ OCH ₃	¹³ CN, C ¹⁸ O, ¹³ CO, C ¹⁵ N, C ¹⁷ O	H (39) α	19
G075.76+00.33	SO, CN, OCS, CCS, t-HCOOH, HC ₃ N	CH ₃ OH, CH ₃ CN, HC ₅ N, CH ₃ CHO, C ₂ H ₅ OH	¹³ CN, C ¹⁸ O, ¹³ CO, C ¹⁵ N, C ¹⁷ O	H (39) α	16
G078.12+03.63	SO, CN, OCS, CCS, HNCO, HC ₃ N	NH ₂ CHO, CH ₃ OH, CH ₃ CN	¹³ CN, C ¹⁸ O, ¹³ CO, C ¹⁵ N, C ¹⁷ O	non-detection	14
G081.75+00.59	SO, CN, OCS, CCS, HNCO, HC ₃ N, t-HCOOH	CH ₃ OH, CH ₃ CN, HC ₅ N, CH ₃ CHO	¹³ CN, C ¹⁸ O, ¹³ CO, C ¹⁵ N, C ¹⁷ O	non-detection	16
G081.87+00.78	SO, CN, OCS, CCS, SO ₂ , HNCO, HOCO ⁺ , t-HCOOH, HC ₃ N	NH ₂ CHO, CH ₃ OH, CH ₃ CN, CH ₃ CHO, CH ₃ OCHO, C ₂ H ₅ CN, C ₂ H ₅ OH, CH ₃ OCH ₃	³⁴ SO, OC ³⁴ S, ¹³ CN, C ¹⁸ O, C ¹⁵ N, ¹³ CO, C ¹⁷ O	non-detection	24
G092.67+03.07	SO, CN, OCS, CCS, HNCO, HC ₃ N, t-HCOOH	CH ₃ OH, CH ₃ CN, CH ₃ CHO, CH ₃ OCH ₃	³⁴ SO, ¹³ CN, C ¹⁸ O, C ¹⁵ N, ¹³ CO, C ¹⁷ O	non-detection	17
G109.87+02.11	SO, CN, OCS, CCS, SO ₂ , HNCO, t-HCOOH, HC ₃ N	CH ₃ OH, CH ₃ CN, HC ₅ N, CH ₃ CHO	³⁴ SO, ¹³ CN, C ¹⁸ O, C ¹⁵ N, ¹³ CO, C ¹⁷ O	non-detection	18
G111.54+00.77	SO, CN, OCS, CCS, SO ₂ , HNCO, HC ₃ N, t-HCOOH	NH ₂ CHO, CH ₃ OH, CH ₃ CN, CH ₃ CHO, CH ₃ OCHO, C ₂ H ₅ OH, CH ₃ OCH ₃	¹³ CN, C ¹⁸ O, C ¹⁵ N, ¹³ CO, C ¹⁷ O	H (39) α, He (39) α, H (55) γ, H (48) β	20
G121.29+00.65	SO, CN, OCS, CCS, HNCO, HC ₃ N, t-HCOOH	CH ₃ OH, CH ₃ CN, HC ₅ N, CH ₃ CHO, CH ₃ OCHO	³⁴ SO, ¹³ CN, C ¹⁸ O, C ¹⁵ N, ¹³ CO, C ¹⁷ O	non-detection	18
G123.06-06.30	SO, CN, OCS, CCS, HNCO, HC ₃ N, t-HCOOH	CH ₃ OH, CH ₃ CN, HC ₅ N, CH ₃ CHO, CH ₃ OCHO, CH ₃ OCH ₃	³⁴ SO, ¹³ CN, C ¹⁸ O, C ¹⁵ N, ¹³ CO, C ¹⁷ O	non-detection	13
G133.94+01.06	SO, CN, OCS, CCS, SO ₂ , HNCO, HOCO ⁺ , t-HCOOH, HC ₃ N	CH ₃ OH, CH ₃ CN, CH ₃ CHO, CH ₃ OCHO, C ₂ H ₅ CN, CH ₃ OCH ₃	OC ³⁴ S, ¹³ CN, OC ³³ S, C ¹⁸ O, ¹³ CO, C ¹⁷ O	H (39) α, H (55) γ, H (48) β	21
G168.06+00.82	SO, CN, HC ₃ N	CH ₃ OH	C ¹⁸ O, ¹³ CO, C ¹⁷ O	non-detection	7
G176.51+00.20	SO, CN, OCS, CCS, HC ₃ N	CH ₃ OH, CH ₃ CN, CH ₃ CHO, CH ₃ OCH ₃	¹³ CN, C ¹⁸ O, C ¹⁵ N, ¹³ CO, C ¹⁷ O	non-detection	14
G183.72-03.66	SO, CN, OCS, CCS, HOCO ⁺ , HC ₃ N	CH ₃ OH, CH ₃ CN, CH ₃ CHO, CH ₃ OCH ₃	¹³ CN, C ¹⁸ O, C ¹⁵ N, ¹³ CO, C ¹⁷ O	non-detection	15
G188.94+00.88	SO, CN, OCS, CCS, HC ₃ N, t-HCOOH	CH ₃ OH, CH ₃ CN, CH ₃ CHO	³⁴ SO, ¹³ CN, C ¹⁸ O, C ¹⁵ N, ¹³ CO, C ¹⁷ O	non-detection	15
G192.60-00.04	SO, CN, OCS, CCS, SO ₂ , HNCO, HC ₃ N, t-HCOOH	NH ₂ CHO, CH ₃ OH, CH ₃ CN, CH ₃ CHO, CH ₃ OCHO, C ₂ H ₅ OH	³⁴ SO, ¹³ CN, C ¹⁸ O, C ¹⁵ N, ¹³ CO, C ¹⁷ O	non-detection	20
G209.00-19.38	SO, CN, OCS, CCS, SO ₂ , HNCO, HC ₃ N	CH ₃ OH, CH ₃ CN, CH ₃ CHO, CH ₃ OCHO, C ₂ H ₅ CN, CH ₃ OCH ₃	¹³ CN, C ¹⁸ O, C ¹⁵ N, ¹³ CO, C ¹⁷ O	H (39) α, He (39) α, H (65) ε, He (55) γ, H (60) δ, H (68) ζ, H (48) β	18
G232.62+00.99	SO, CN, OCS, CCS, HNCO, HC ₃ N	CH ₃ OH, CH ₃ CN	³⁴ SO, ¹³ CN, C ¹⁸ O, ¹³ CO, C ¹⁷ O	non-detection	13

Note. Values of N* do not include radio recombination lines.

Table 4. Detected lines and their parameters in each sources

Species	Transitions	Rest Freq. (MHz)	E_u (K)	$\mu^2 S$ (D ²)	T_{mb} (mK)	V_{LSR} (km s ⁻¹)	ΔV (km s ⁻¹)	$\int T_{mb} dv$ (mK km s ⁻¹)
(1)	(2)	(3)	(4)	(5)	(6)	(7)	(8)	(9)
G000.67-00.03								
NH ₂ CHO	5(2, 4) - 4(2, 3)	105972.665(37e-3)	27.2	54.915	611	62.5(0.1)	13.2 (0.3)	8594(140)
NH ₃ CHO	5(4, 1) - 4(4, 0)	106107.870(88e-3)	63.0	23.537	239	62.5(0.3)	9.3(0.7)	2360(138)
NH ₂ CHO	5(3, 3) - 4(3, 2)	106134.468(55e-3)	42.1	41.845	391	62.5(0.5)	12.8(0.5)	5319(171)
NH ₂ CHO	5(3, 2) - 4(3, 1)	106141.442(55e-3)	42.1	41.84	375	62.5(0.5)	12.0(0.5)	4791(160)
NH ₂ CHO	5(2, 3) - 4(2, 2)	106541.773(37e-3)	27.2	54.915	598	62.5(0.1)	12.8(0.3)	8163(172)
C ₂ S	8(9) - 7(8)	106347.726(2e-2)	25.0	74.425	340	62.0(0.2)	17.4(0.6)	6309(164)
C ₂ H ₅ CN	15(3, 12) - 15(2, 13)	106375.033(5e-2)	61.7	13.244	46	62.0(1.1)	9.2(3.1)	453(110)
HC ₅ N	40 - 39	106498.910(7e-3)	104.8	2249.7	90	62.0(0.1)	18.7(0.5)	1802(77)
C ₂ H ₃ CN	11(1, 10) - 10(1, 9)	106641.383(1e-3)	32.9	476.24	204	62.5(0.3)	12.6(0.8)	2745(168)
C ₂ H ₅ OH	13(1, 12) - 13(0, 13)	106649.479(5e-2)	79.4	10.463	42	62.0(1.8)	16.1(10.3)	719(265)
C ₂ H ₅ OH	6(1, 5) - 5(1, 4)	106676.542(5e-2)	76.1	9.325	40	62.0(1.5)	8.1(2.4)	345(109)
C ₂ H ₅ OH	9(2, 8) - 9(1, 9)	106723.558(5e-2)	42.7	7.9044	108	62.0(0.5)	18.0(0.5)	2078(66)
H α	H (39) α	106737.357(0)	—	—	265	55.6(0.6)	40.8(1.4)	10701 (294)
C ₂ H ₅ OH	6(1, 5) - 5(1, 4)	106767.234(5e-2)	80.7	9.6466	56	62.0(1.5)	21.9(6.3)	1890(350)
CH ₃ OCH ₃	9(1, 8) - 8(2, 7)	106777.344(9e-3)	43.4	58.573	89	62.0(0.9)	10.7(1.8)	1006(159)
OC ³⁴ S	9 - 8	106787.390(2e-3)	25.6	4.601	146	62.0(0.5)	10.6(1.1)	1643(147)
CH ₃ OH, vt=0-2	3(1) ⁺ - 4(0) ⁺ , vt=0	107013.831(1e-2)	28.3	12.036	1321	60.0(0.1)	11.8(0.1)	16553(143)
C ₂ H ₅ CN	12(2, 11) - 11(2, 10)	107043.527(5e-2)	37.9	172.86	248	62.0(0.3)	12.1(0.7)	3182(148)
CH ₃ C ¹⁵ N	6(3) - 5(3)	107043.140(6e-2)	82.4	277.350	blended	—	—	—
CH ₃ C ¹⁵ N	6(0) - 5(0)	107061.410(6e-2)	18.0	184.936	139	61.8(0.5)	15.2(1.3)	2250(165)
CH ₃ OH, vt=0-2	15(-2) - 15(1) E2, vt=0	107159.906(14e-3)	304.7	10.421	180	60.0(0.5)	33.5(1.3)	6402(205)
¹³ CH ₃ CN	6(2) - 5(2)	107188.500(1e-1)	46.6	164.068	231	61.5 (0.5)	14.5(1.1)	3552(240)
¹³ CH ₃ CN	6(1) - 5(1)	107194.550(1e-1)	25.2	179.427	134	61.5(0.7)	10.1(2.0)	1435(231)
¹³ CH ₃ CN	6(0) - 5(0)	107196.570(1e-1)	18.0	184.590	120	61.5(0.5)	15.3(2.3)	1959(184)
C ₂ H ₅ CN	12(7, 5) - 11(7, 4)	107485.160(5e-2)	88.0	117.36	272	62.0(0.5)	16.7(0.5)	4830(59)
C ₂ H ₅ CN	12(6, 6) - 11(6, 5)	107486.949(5e-2)	73.6	133.42	160	62.0(0.5)	11.0(0.5)	1866(59)
C ₂ H ₅ CN	12(5, 7) - 11(5, 6)	107502.432(5e-2)	61.3	146.99	241	62.0(0.5)	16.1(0.5)	4140(59)
C ₂ H ₅ CN	12(10, 2) - 11(10, 1)	107519.861(5e-2)	144.6	54.355	130	62.0(0.5)	10.6(0.5)	1466(59)
CH ₃ OCHO	9(2, 8) - 8(2, 7) E	107537.258(1e-2)	28.8	22.60702	159	62.0(0.5)	13.2(0.5)	2218(59)
CH ₃ OCHO	9(2, 8) - 8(2, 7) A	107543.711(1e-2)	28.8	22.61344	blended	—	—	—
C ₂ H ₅ CN	12(4, 9) - 11(4, 8)	107544.042(5e-2)	51.3	158.12	302	62.0(0.5)	10.1(0.5)	3251(59)
C ₂ H ₅ CN	12(4, 8) - 11(4, 7)	107547.460(5e-2)	51.3	158.11	183	62.0(0.5)	10.5(0.5)	2046(59)
C ₂ H ₅ CN	12(3, 10) - 11(3, 9)	107594.056(5e-2)	43.6	166.77	213	62.0(0.5)	16.6(0.5)	3770(59)
CH ₃ OCHO	23(6, 17) - 23(5, 18) E	107604.366(1e-2)	189.0	7.68978	68	62.0(0.5)	8.6(0.5)	626(59)
C ₂ H ₅ CN	12(3, 9) - 11(3, 8)	107734.723(5e-2)	43.6	166.76	221	62.0(0.5)	26.9(1.8)	6317(271)
CH ₃ OCH ₃	47(18, 30) - 48(17, 32)	107770.696(68)	1479.8	24.31526	68	62.0(0.7)	6.7(1.4)	479(97)
SO ₂	12(4, 8) - 13(3, 11)	107843.470(2e-3)	111.0	4.5354	175	60.0(0.5)	16.6 (1.0)	3096(163)
t-HCOOH	5(1, 5) - 4(1, 4)	108126.720(3e-3)	18.8	9.6966	114	62.0(0.6)	13.4(1.5)	1636(151)
CH ₃ SH, v=0-2	4(-1, 4) - 4(0, 4) A, vt=0	108379.758(1e-3)	17.3	0.3856	51	62.0(1.2)	4.4(2.1)	237(121)
CH ₃ OH, vt=0-2	0(0) - 1(-1) E2, vt=0	108893.945(12e-3)	13.1	3.9134	860	62.0(0.1)	11.7(0.2)	10689(171)
SiS	6(0) - 5(0)	108924.301(1e-2)	18.3	5.62	138	62.0(0.6)	17.2(2.0)	2530(200)
C ₂ H ₅ CN	12(2, 10) - 11(2, 9)	108940.554(5e-2)	38.2	172.93	blended	—	—	—
C ₂ H ₅ CN	11(3, 9) - 12(0, 12)	108940.696(4e-3)	38.4	0.042598	246	62.0(0.3)	15.2(1.2)	3999(206)
HC ₃ N	12 - 11	109173.634(1e-2)	34.1	167.1	5943	62.0(0.5)	17.0(0.5)	107590(914)
SO	3(2) - 2(1)	109252.220(1e-1)	21.1	3.5585	2083	62.0(0.0)	20.4(0.1)	45302(340)
HC ₃ N, v ₇ =1	12(-1) - 11(1)	109442.013(2e-2)	355.0	165.12	136	62.0(0.7)	25.7(2.0)	3725(228)
OCS	9 - 8	109463.063(5e-3)	26.3	4.6034	1574	62.0(0.1)	11.2(0.3)	18740(647)
HNCO	5(1, 5) - 4(1, 4)	109495.996(6e-3)	59.0	11.847	409	62.0(0.3)	16.2(0.9)	7058(298)
CH ₃ OCH ₃	8(2, 7) - 8(1, 8) AA	109576.778(11e-3)	38.3	59.669	97	62.0(1.4)	33.8(5.2)	3505(370)
HC ₃ N, v ₇ =1	12(-1) - 11(1)	109442.013(2e-2)	355.0	165.12	172	62.0(0.8)	27.8(2.8)	6910(366)
C ₂ H ₅ CN	12(1, 11) - 11(1, 10)	109650.263(5e-2)	53.4	176.49	246	62.0(0.4)	19.4(1.5)	5084(274)
NH ₂ CHO	5(1, 4) - 4(1, 3)	109753.549(25e-3)	18.8	62.756	687	62.5(0.5)	15.1(0.5)	11021(454)
C ¹⁸ O	1 - 0	109782.173(6e-3)	5.3	0.01221	3271	62.0(0.5)	11.2(0.5)	72371(454)
HNCO	5(0, 5) - 4(0, 4)	109905.749(7e-3)	15.8	12.482	4931	62.0(0.1)	22.6(0.1)	118770(478)
¹³ CO	1 - 0	110201.35(0)	5.3	0.01220	10745	63.0(0.5)	20.1(0.9)	229350(11600)
HNCO	5(1, 4) - 4(1, 3)	110298.089(5e-3)	59.2	11.847	425	62.0(0.5)	18.3(0.5)	8291(430)
CH ₃ ¹³ CN	6(2) - 5(2)	110320.400(1e-1)	47.1	164.054	146	62.2(0.5)	14.2(0.5)	2210(430)
CH ₃ ¹³ CN	6(1) - 5(1)	110326.770(1e-1)	25.7	179.434	170	62.1(0.5)	16.0(0.5)	2890(430)
CH ₃ ¹³ CN	6(0) - 5(0)	110328.870(1e-1)	18.5	184.563	330	62.2(0.5)	19.4(0.5)	6808(430)
CH ₃ CN	6(5, 0) - 5(5, 0)	110330.345(0)	197.1	56.399	blended	—	—	—
CH ₃ CN	6(4, 0) - 5(4, 0)	110349.471(0)	132.8	102.54	455	62.0(0.5)	24.1(0.5)	11703(430)
CH ₃ CN	6(3, 0) - 5(-3, 0)	110364.354(0)	82.8	138.45	1485	62.0(0.5)	18.1(0.5)	28546(430)
CH ₃ CN	6(-3, 0) - 5(3, 0)	110364.354(0)	82.8	138.45	blended	—	—	—
CH ₃ CN	6(2, 0) - 5(2, 0)	110374.989(0)	47.1	164.06	1800	62.0(0.5)	15.0(0.5)	28663(430)
CH ₃ CN	6(1, 0) - 5(1, 0)	110381.372(0)	25.7	179.45	3010	62.0(0.5)	17.8(0.5)	57045(430)
CH ₃ OCHO	9(7, 3) - 8(7, 2) E	110536.003(1e-2)	59.1	9.46692	89	62.0(0.8)	10.2(2.9)	974(186)
CH ₃ OCHO	9(6, 3) - 8(6, 2) E	110652.813(1e-2)	50.5	13.30853	74	62.0(1.5)	25.6(4.7)	2003(283)
CH ₃ OCHO	9(6, 3) - 8(6, 2) A	110663.429(1e-2)	50.4	13.31127	191	62.0(0.6)	13.0(1.0)	2648(205)
CH ₃ OCHO	9(6, 4) - 8(6, 3) A	110663.273(1e-2)	50.4	13.3112	blended	—	—	—
CH ₃ OCHO	10(1, 10) - 9(1, 9) A	110790.526(1e-2)	30.3	16.17539	236	62.0(0.2)	5.4(0.2)	1351(17)
C ₂ H ₅ CN	12(1, 12) - 11(1, 11)	110839.968 (1e-3)	36.8	520.3	174	62.5(0.2)	6.0(0.2)	1116(17)
CH ₃ OCHO	9(5, 4) - 8(5, 3) E	110873.955(1e-2)	43.2	16.55225	97	62.0(0.2)	4.3(0.2)	448(17)
CH ₃ OCHO	9(5, 5) - 8(5, 4) E	110882.331(1e-2)	43.2	16.55225	212	62.0(0.2)	5.5(0.2)	1247(17)
CH ₃ OCHO	9(3, 7) - 8(3, 6) A	110887.092(1e-2)	32.6	21.25577	144	62.0(0.2)	6.5(0.2)	995(17)
CH ₃ OCHO	9(4, 6) - 8(4, 5) E	111223.491(1e-2)	37.2	18.18412	108	62.0(0.7)	9.7(2.4)	1116(184)
CH ₃ OH, vt=0-2	7(2) ⁺ - 8(1) ⁺ , vt=0	111289.453(13e-3)	102.7	9.3425	368	60.0(0.2)	11.7(0.5)	4601(169)
CH ₃ OCHO	9(4, 5) - 8(4, 4) E	111408.412(1e-2)	37.3	18.18412	91	62.0(0.1)	8.8(1.2)	857(84)
CH ₃ OCHO	9(4, 5) - 8(4, 4) A	111453.300(1e-2)	37.2	19.21778	129	62.0(0.5)	10.3(1.4)	1420(156)
CH ₃ OCHO	9(1, 8) - 8(1, 7) E	111674.131(1e-2)	28.1	23.18984	169	62.0(0.8)	17.3(2.8)	2941(333)
CH ₃ OCHO	9(1, 8) - 8(1, 7) A	111682.189(1e-2)	28.1	23.19587	166	62.0(0.8)	14.1(1.9)	2494(306)
t-HCOOH	5(0, 5) - 4(0, 4)	111746.784(3e-3)	16.1	10.092	153	62.0(0.7)	18.3(2.0)	2988(255)
CH ₃ OCH ₃	19(3, 16) - 19(2, 17) AA	111744.238(29e-3)	187.5	259.8	blended	—	—	—
CH ₃ OCH ₃	7(0, 7) - 6(1, 6) AA	111782.562(8e-3)	25.2	68.407	328	62.0(0.2)	11.6(0.6)	4067(196)
CH ₃ OCH ₃	18(3, 15) - 18(2, 16) EE	111813.668(21e-3)	169.8	386.29	69	62.0(1.5)	15.1(3.7)	1100(230)
HC ₅ N	42 - 41	111823.024(0)	115.4	2362.2	102	62.0(1.0)	10.9(2.3)	1180(203)
H β	H (48) β	111885.070(0)	—	—	56	64.1(1.9)	14.8(3.7)	881(208)
CH ₃ CHO	6(1, 6) - 5(1, 5) A, vt=0	112248.716(3e-3)	21.1	73.76807	385	62.0(0.5)	27.4(0.5)	11227(131)

Table 4. (Continued)

Species	Transitions	Rest Freq.	E_u	$\mu^2 S$	T_{mb}	V_{LSR}	ΔV	$\int T_{mb} dv$
(1)	(2)	(MHz)	(K)	(D^2)	(mK)	($km s^{-1}$)	($km s^{-1}$)	($mK km s^{-1}$)
		(3)	(4)	(5)	(6)	(7)	(8)	(9)
C ₂ H ₃ CN	12(0,12) – 11(0,11)	112840.637(1e-3)	35.3	523.56	245	62.5(0.5)	14.0(0.5)	2660(59)
t-HCOOH	5(2,3) – 4(2,2)	112891.443(3e-3)	28.9	8.4849	134	62.0(0.5)	7.9(0.5)	1124(59)
CH ₃ OCH ₃	17(3,14) – 17(2,15) AA	113061.072(22e-3)	153.1	221.33	89	62.0(0.5)	13.4(0.5)	1270(123)
C ₂ H ₅ OH	10(2,9) – 10(1,10)	113098.078(5e-2)	51.0	8.3566	99	62.0(0.5)	20.4(0.5)	2140(123)
CN	N=1-0, J=1/2-1/2, F=1/2-1/2	113123.370(6e-3)	5.4	0.15271	blended	–	–	–
CN	N=1-0, J=1/2-1/2, F=1/2-3/2	113144.157(6e-3)	5.4	1.2492	275	60.0(0.5)	13.2(0.5)	3874(117)
CN	N=1-0, J=1/2-1/2, F=3/2-1/2	113170.492(4e-3)	5.4	1.2199	609	59.3(0.6)	9.6(1.3)	6273(683)
CN	N=1-0, J=1/2-1/2, F=3/2-3/2	113191.279(3e-3)	5.4	1.5836	252	59.6(0.5)	12.3(0.5)	3303(117)
CCS	9(8) – 8(7)	113410.186(2e-2)	33.6	65.427	178	62.8(0.5)	12.8(0.5)	2434(191)
CN	N=1-0, J=3/2-1/2, F=3/2-1/2	113488.120(3e-3)	5.4	1.5838	272	60.3(0.8)	7.8(2.3)	2258(502)
CN	N=1-0, J=3/2-1/2, F=5/2-3/2	113490.970(2e-3)	5.4	4.205	186	60.0(1.3)	7.0(3.0)	1375(467)
CN	N=1-0, J=3/2-1/2, F=1/2-1/2	113499.644(3e-3)	5.4	1.2491	168	60.0(1.3)	7.1(2.6)	1263(429)
CN	N=1-0, J=3/2-1/2, F=3/2-3/2	113508.907(3e-3)	5.4	1.2196	123	59.8(1.5)	4.5(3.3)	585(356)
CN	N=1-0, J=3/2-1/2, F=1/2-3/2	113520.432(4e-3)	5.4	0.15263	260	60.1(0.9)	6.6(2.3)	1815(471)
							
							
							
							
			G232.62+00.99					
CCS	8(9) – 7(8)	106347.726(2e-2)	25.0	74.425	54	18.0(0.1)	2.8(0.3)	159(14)
³⁴ SO	3(2) – 2(1)	106743.244(7e-2)	20.9	3.557	39	16.3(0.1)	2.4(0.4)	100(12)
CH ₃ OH, vt=0-2	3(1) ⁺ – 4(0) ⁺ , vt=0	107013.831(1e-2)	28.3	12.036	28	18.0(0.3)	2.8(0.5)	81(13)
¹³ CN	1(1,0) – 0(1,1), F = 1 – 2	108426.889(5e-2)	5.2	1.267	12	16.1(0.5)	4.3(1.2)	56(13)
¹³ CN	1(1,1) – 0(1,0), F = 0 – 1	108631.121(5e-2)	5.2	0.642	17	16.3(0.2)	1.2(0.5)	23(7)
¹³ CN	1(1,1) – 0(1,0), F = 1 – 1	108636.923(5e-2)	5.2	1.932	99	16.4(0.7)	5.0(1.5)	53(15)
¹³ CN	1(2,1) – 0(1,1), F = 1 – 0	108638.212(5e-2)	5.2	0.722	14	16.6(0.4)	2.1(0.9)	31(10)
¹³ CN	1(2,1) – 0(1,1), F = 2 – 1	108643.590(5e-2)	5.2	0.856	12	16.2(0.7)	5.5(1.4)	71(16)
¹³ CN	1(2,1) – 0(1,1), F = 0 – 1	108644.346(5e-2)	5.2	0.642	blended	–	–	–
¹³ CN	1(2,1) – 0(1,1), F = 1 – 1	108645.064(5e-2)	5.2	0.551	blended	–	–	–
¹³ CN	1(1,1) – 0(1,0), F = 2 – 1	108651.297(5e-2)	5.2	3.276	20	16.8(0.4)	4.7(1.2)	101(17)
¹³ CN	1(2,1) – 0(1,1), F = 2 – 2	108657.646(5e-2)	5.2	2.420	28	17.1(0.2)	2.5(0.4)	74(10)
¹³ CN	1(2,1) – 0(1,1), F = 1 – 2	108658.948(5e-2)	5.2	0.669	blended	–	–	–
¹³ CN	1(2,2) – 0(1,1), F = 3 – 2	108780.201(5e-2)	5.2	4.905	29	16.4(0.2)	4.4(0.6)	137(15)
¹³ CN	1(2,2) – 0(1,1), F = 2 – 1	108782.374(5e-2)	5.2	2.586	35	16.6(0.1)	1.8(0.2)	66(9)
¹³ CN	1(2,2) – 0(1,1), F = 1 – 0	108786.982(5e-2)	5.2	1.144	19	17.2(0.1)	0.8(0.4)	17(7)
¹³ CN	1(2,2) – 0(1,1), F = 1 – 1	108793.753(5e-2)	5.2	0.894	11	16.8(0.4)	2.3(0.8)	27(9)
¹³ CN	1(2,2) – 0(1,1), F = 2 – 2	108796.400(5e-2)	5.2	0.918	12	17.1(0.3)	1.3(0.6)	17(7)
CH ₃ OH, vt=0-2	0(0) – 1(-1) E2, vt=0	108893.945(12e-3)	13.1	3.9134	81	18.1(0.1)	4.9(0.2)	423(17)
HC ₃ N	12 – 11	109173.634(1e-2)	34.1	167.1	1244	17.0(0.1)	2.1(0.1)	2834(25)
SO	3(2) – 2(1)	109252.220(1e-1)	21.1	3.5585	558	17.1(0.1)	3.0(0.1)	1803(19)
OCS	9 – 8	109463.063(5e-3)	26.3	4.6034	36	16.8(0.3)	3.2(1.0)	123(23)
C ¹⁸ O	1 – 0	109782.173(6e-3)	5.3	0.01221	1166	16.0(0.1)	3.4(0.1)	4251(6)
HNCO	5(0,5) – 4(0,4)	109905.749(7e-3)	15.8	12.482	50	16.5(0.4)	1.4(0.9)	75(45)
¹³ CO	1 – 0	110201.35(0)	5.3	0.01220	11589	16.2(0.1)	4.3(0.1)	53250(79)
CH ₃ CN	6(5,0) – 5(5,0)	110330.345(0)	197.1	56.399	27	17.2(0.5)	3.9(0.5)	112(11)
CH ₃ CN	6(4,0) – 5(4,0)	110349.471(0)	132.8	102.54	16	17.2(0.5)	9.4(0.5)	160(11)
CH ₃ CN	6(3,0) – 5(3,0)	110364.354(0)	82.8	138.45	36	17.1(0.5)	3.0(0.5)	115(11)
CH ₃ CN	6(-3,0) – 5(3,0)	110364.354(0)	82.8	138.45	blended	–	–	–
CH ₃ CN	6(2,0) – 5(2,0)	110374.989(0)	47.1	164.06	43	17.2(0.5)	6.2(0.5)	280(11)
CH ₃ CN	6(1,0) – 5(1,0)	110381.372(0)	25.7	179.45	88	17.2(0.4)	3.5(0.5)	329(11)
CH ₃ CN	6(0,0) – 5(0,0)	110383.500(0)	18.5	184.58	119	17.2(0.5)	2.7(0.5)	345(11)
C ¹⁷ O	1 – 0	112359.284(1e-3)	5.4	0.01217	129	15.8(0.9)	2.6(1.7)	356(197)
CN	N=1-0, J=1/2-1/2, F=1/2-1/2	113123.370(6e-3)	5.4	0.15271	167	17.0(0.5)	2.8(0.5)	501(75)
CN	N=1-0, J=1/2-1/2, F=1/2-3/2	113144.157(6e-3)	5.4	1.2492	759	17.1(0.5)	3.6(0.5)	2927(75)
CN	N=1-0, J=1/2-1/2, F=3/2-1/2	113170.492(4e-3)	5.4	1.2199	815	17.0(0.5)	3.4(0.5)	2932(75)
CN	N=1-0, J=1/2-1/2, F=3/2-3/2	113191.279(3e-3)	5.4	1.5836	889	17.1(0.5)	3.4(0.5)	3249(75)
CN	N=1-0, J=3/2-1/2, F=3/2-1/2	113488.120(3e-3)	5.4	1.5838	834	17.0(0.5)	3.5(0.5)	3121(163)
CN	N=1-0, J=3/2-1/2, F=5/2-3/2	113490.970(2e-3)	5.4	4.205	1721	17.0(0.5)	4.1(0.5)	7456(163)
CN	N=1-0, J=3/2-1/2, F=1/2-1/2	113499.644(3e-3)	5.4	1.2491	569	17.0(0.4)	4.1(0.5)	2476(163)
CN	N=1-0, J=3/2-1/2, F=3/2-3/2	113508.907(3e-3)	5.4	1.2196	701	17.0(0.5)	3.4(0.5)	2521(163)
CN	N=1-0, J=3/2-1/2, F=1/2-3/2	113520.432(4e-3)	5.4	0.15263	105	17.0(0.7)	8.3(0.5)	920(163)

Note. This is only a subset of the whole table, which is available in the supplementary material.

- (1): Molecule name; (2): Transition quantum numbers; (3): Rest frequency; (4): Upper state energy level (K);
- (5): Dipole-weighted transition dipole matrix elements; (6): Peak intensity; (7): centroid velocity; (8): FWHM;
- (9): Integrated intensity. "–" represents no values.

Table 5. Detected H (39) α and He (39) α .

Sources	RRL	Rest Freq. (MHz)	V_{LSR} (km s $^{-1}$)	ΔV (km s $^{-1}$)	$\int T_{mb} dv$ (mK km s $^{-1}$)
G000.67–00.03	H (39) α	106737.357(0)	55.6(0.6)	40.8(1.4)	10701 (294)
G005.88–00.39	H (39) α	106737.357(0)	6.9(0.2)	59.1(0.6)	67990(543)
G009.62+00.19	H (39) α	106737.357(0)	7.9(0.7)	19.6(1.8)	1342(98)
	He (39) α	106780.852(0)	8.2(1.0)	9.2(1.8)	319(63)
G010.62–00.38	H (39) α	106737.357(0)	2.3(0.1)	45.0(2.5)	12209(1590)
	He (39) α	106780.852(0)	2.3(0.1)	45.0(2.5)	12209(1590)
G012.80–00.20	H (39) α	106737.357(0)	37.2(0.5)	33.5(0.5)	81558(386)
	He (39) α	106780.852(0)	37.1(0.2)	33.0(0.7)	7541(116)
G015.03–00.67	H (39) α	106737.357(0)	15.4(0.2)	37.5(0.3)	33252(244)
	He (39) α	106780.852(0)	15.4(0.7)	36.2(1.5)	3316(131)
G023.44–00.18	H (39) α	106737.357(0)	95.9(1.4)	14.5(2.5)	312(58)
G027.36–00.16	H (39) α	106737.357(0)	105.5(1.5)	17.3(3.7)	379(65)
G029.95–00.01	H (39) α	106737.357(0)	95.9(0.2)	29.8(0.4)	16016(190)
G031.28+00.06	H (39) α	106737.357(0)	115.5(0.8)	20.2(1.9)	1029(85)
G035.20–01.73	H (39) α	106737.357(0)	47.1(0.3)	25.2(0.6)	3753(82)
G043.16+00.01	H (39) α	106737.357(0)	8.2(0.1)	36.2(0.2)	50729(338)
	He (39) α	106780.852(0)	8.1(0.9)	28.4(2.1)	3569(239)
G043.79–00.12	H (39) α	106737.357(0)	65.9(1.7)	43.7(4.1)	996(82)
G049.48–00.36	H (39) α	106737.357(0)	55.4(0.5)	29.4(0.5)	40170(210)
	He (39) α	106780.852(0)	56.7(0.5)	25.5(0.8)	4537(51)
G049.48–00.38	H (39) α	106737.357(0)	59.4(0.5)	26.9(0.5)	14554(107)
G069.54–00.97	H (39) α	106737.357(0)	3.8(0.6)	32.5(1.7)	2003(82)
G075.76+00.33	H (39) α	106737.357(0)	-15.1(0.5)	30.8(1.6)	2730(105)
G111.54+00.77	H (39) α	106737.357(0)	-63.7(0.2)	26.6(0.7)	4432(182)
G133.94+01.06	H (39) α	106737.357(0)	-47.6(0.5)	33.2(0.2)	23203(105)
G209.00–19.38	H (39) α	106737.357(0)	-1.4(0.)	25.1(0.1)	26798(76)
	He (39) α	106780.852(0)	-2.2(0.9)	17.4(2.3)	2126(257)

Table 6. Observational parameters of the remaining unidentified lines.

Sources	ν_{obs} (MHz)	ΔV (km s ⁻¹)	$\int T_{\text{mb}} dv$ (mK km s ⁻¹)	Sources	ν_{obs} (MHz)	ΔV (km s ⁻¹)	$\int T_{\text{mb}} dv$ (mK km s ⁻¹)
G000.67-00.03	107606.336	9.6(2.3)	595(128)	G049.48-0.36	111503.390	5.9(1.3)	418(63)
	107623.459	13.3(2.0)	758(126)		111518.493	8.9(1.4)	503(68)
	110607.218	4.8(1.5)	564(128)		112579.794	1.9(1.0)	109(41)
	111322.089	13.4(1.9)	1767(195)		112581.764	4.2(0.8)	362(52)
	111347.774	6.0(1.7)	491(125)	G049.48-00.38	105869.777	9.6(3.1)	1009(107)
	111384.760	9.3(1.6)	952(150)		105882.363	7.1(2.1)	205(52)
	111600.856	1.2(0.8)	132(59)		105894.692	6.1(0.9)	460(53)
	111602.808	1.8(0.9)	197(135)		106333.887	7.2(0.5)	355(19)
	111604.350	5.1(1.5)	507(163)		106354.418	8.1(0.5)	452(19)
	113136.810	15.5(0.5)	12674(117)		106365.908	7.6(0.5)	275(19)
	113156.968	9.1(0.9)	7814(686)		106388.510	5.6(0.5)	154(19)
	113175.058	4.1(0.7)	2100(355)		106610.411	5.5(0.5)	719(30)
	113195.733	7.5(2.2)	1282(430)		107570.762	9.3(5.8)	2606(220)
	113455.777	19.0(0.3)	1346(285)		107607.706	8.5(2.5)	302(84)
G009.62+00.19	108576.858	5.2(0.4)	708(53)		107624.486	12.3(1.7)	712(98)
	108976.164	2.8(0.5)	425(67)		107906.336	6.3(2.5)	206(56)
	108977.192	2.1(0.5)	282(67)		107920.719	4.1(0.9)	152(34)
	109376.524	4.5(1.0)	920(275)		107932.021	9.3(2.3)	361(62)
	109377.140	3.3(0.5)	510(256)		107941.610	6.1(1.2)	211(41)
	109726.730	2.0(0.2)	275(31)		107965.069	7.1(0.3)	1527(56)
	110145.582	1.5(0.1)	2087(43)		107968.493	6.1(0.6)	574(52)
	112776.421	3.2(0.4)	579(57)		108332.534	10.8(1.7)	472(62)
G010.47+00.02	105866.181	3.5(1.1)	212(134)		108359.418	11.1(5.0)	387(102)
	105867.500	6.4(1.6)	634(156)		109510.959	9.2(0.5)	1710(63)
	110996.712	7.0(1.1)	873(94)		109588.185	6.2(0.5)	1307(63)
	111004.726	11.6(1.1)	3286(94)		110598.493	8.7(1.3)	2336(296)
	111008.733	7.3(1.1)	1438(94)		111007.534	11.0(1.6)	802(94)
	111014.743	10.8(1.1)	1590(94)		111025.000	10.0(1.5)	559(83)
	111022.312	13.7(1.1)	3227(94)		111456.849	7.1(0.5)	249(65)
	111064.384	7.6(1.1)	2123(94)		111486.027	12.4(0.5)	807(65)
G010.62-00.38	112774.349	4.7(0.5)	1578(150)		111504.658	3.2(1.0)	165(45)
G011.49-01.48	110583.570	1.9(0.4)	349(59)		111558.288	11.7(1.4)	922(90)
	110585.497	1.6(0.4)	218(48)		111681.798	9.4(1.1)	1295(241)
G011.91-00.61	106900.685	7.0(0.9)	492(46)		111687.586	7.7(1.1)	603(241)
	110588.990	0.9(0.4)	70(29)		111733.219	17.6(1.1)	1999(241)
	110591.473	2.8(0.5)	520(72)		111906.884	6.9(1.8)	399(74)
	110593.099	3.3(0.3)	447(76)		112014.726	9.9(1.8)	900(139)
	112786.165	3.1(0.6)	408(56)		112095.205	6.0(0.5)	457(47)
G012.80-00.20	112785.891	3.6(0.3)	928(60)		112122.740	7.8(0.5)	4215(47)
G012.88+00.48	110587.877	0.7(0.5)	71(24)		112146.986	4.9(0.5)	393(47)
	110590.480	2.5(0.5)	589(24)		112158.082	4.6(0.5)	375(47)
	110592.329	3.2(0.5)	400(24)		112792.945	5.1(0.7)	1238(157)
	111396.439	2.7(0.5)	237(45)		113535.873	5.2(1.0)	450(77)
	112785.240	2.3(0.2)	481(42)		113579.863	4.3(0.8)	380(67)
G012.90-00.24	110158.493	2.4(1.1)	810(283)	G059.78+00.06	108588.082	3.3(0.9)	102(23)
	110591.986	3.4(1.1)	406(122)		108592.534	1.2(0.5)	35(13)
	110593.630	3.3(2.0)	241(128)		110585.548	1.2(0.5)	169(40)
G012.90-00.26	106900.480	4.9(0.9)	325(43)		110588.116	2.2(0.5)	732(40)
	110589.332	2.2(0.7)	165(50)		110589.897	1.7(0.5)	402(40)
	110591.986	3.3(0.3)	1123(80)		112782.706	1.5(0.3)	178(27)
	110593.699	3.6(0.5)	677(83)	G069.54-00.97	106909.315	5.1(0.8)	329(37)
	112786.507	2.8(0.3)	604(48)		107011.849	3.4(1.5)	118(36)
G014.33-00.64	106905.462	3.0(1.0)	222(59)		107013.630	1.9(0.3)	186(23)
	110151.644	1.8(0.3)	372(52)		110582.192	2.0(0.8)	121(42)
	110584.966	2.6(0.4)	379(56)		110584.760	3.2(0.3)	817(56)
	110587.534	3.1(0.1)	1740(62)		110586.473	2.7(0.4)	386(51)
	110589.332	2.6(0.2)	969(60)		112779.452	2.5(0.2)	318(30)
	112782.021	2.4(0.3)	753(70)	G075.76+00.33	110580.470	3.5(0.5)	576(66)
G015.03-00.67	110487.500	2.5(1.0)	128(44)		110582.192	2.7(0.6)	231(54)
	110492.723	2.9(1.4)	98(44)		112775.171	2.5(0.5)	238(43)
	112780.993	1.9(0.4)	386(58)	G078.12+03.63	110577.226	1.2(0.5)	116(22)
G016.58-00.05	110204.281	3.7(0.5)	465(56)		110579.794	2.1(0.5)	765(22)
	110599.144	3.0(0.2)	596(45)		110581.507	1.7(0.5)	411(22)
	110600.890	2.3(0.3)	264(38)		112774.486	2.0(0.3)	361(41)
	112793.425	2.4(0.4)	387(54)	G081.75+00.59	106914.966	1.9(0.5)	86(18)
G023.00-00.41	106885.959	4.7(0.9)	320(41)		108976.541	5.9(0.7)	248(25)
	110604.794	3.9(0.7)	890(127)		109376.199	5.3(0.5)	296(25)
	110606.507	2.9(0.8)	449(111)		109576.267	5.7(0.5)	407(34)
	112798.853	2.1(0.3)	312(40)		110577.226	2.1(0.5)	341(30)
G023.44-00.18	106877.312	3.0(0.5)	221(31)		110578.596	1.9(0.5)	356(30)
	110612.500	6.3(1.1)	824(118)		110579.795	2.9(0.5)	1400(30)
	111745.377	7.5(0.9)	707(65)		110581.507	2.1(0.5)	695(30)
G027.36-00.16	106881.045	4.9(0.5)	268(27)		112773.288	2.6(0.8)	150(34)
	108529.281	11.2(1.1)	372(15)		112774.486	2.2(0.2)	405(31)
	108534.760	15.5(1.1)	557(15)	G081.87+00.78	112741.781	1.7(0.5)	86(18)
	110606.678	2.1(0.4)	227(34)		112778.253	1.8(0.2)	201(16)
	110609.247	3.8(0.2)	1015(48)	G092.67+03.07	106915.514	4.5(0.4)	133(26)
	110610.959	2.6(0.4)	347(43)		110576.541	1.9(0.3)	142(20)
	112108.271	9.2(1.1)	626(22)		110579.281	2.6(0.1)	600(24)
	112710.274	3.5(1.2)	152(42)		110580.822	2.3(0.2)	378(23)
	112766.609	2.9(1.2)	89(34)		112773.801	1.7(0.2)	295(26)
	112772.260	6.9(1.6)	249(54)	G109.87+02.11	110574.658	3.2(0.6)	127(23)
G028.86+00.06	112806.849	2.4(0.4)	270(39)		110577.397	3.4(0.2)	513(27)
G029.95-00.01	110209.503	1.9(0.3)	292(37)		110579.110	2.6(0.3)	246(23)
	111578.459	2.5(0.5)	601(24)		112772.089	3.4(0.4)	394(37)
G031.28+00.06	106874.623	2.4(0.8)	119(36)	G121.29+00.65	106919.863	2.3(0.2)	172(11)
G031.58+00.07	110608.219	2.5(1.1)	112(22)		110572.603	2.2(0.5)	160(16)
	110610.787	3.8(1.1)	448(22)		110575.171	2.7(0.5)	709(16)
	110612.500	2.6(1.1)	210(22)		110576.884	2.3(0.5)	386(16)
G032.04+00.05	106879.589	3.6(0.2)	423(21)		112770.034	2.3(0.1)	335(17)
	110607.877	3.0(0.4)	185(27)	G123.06-06.30	106924.384	3.5(0.2)	295(14)
	110610.445	3.1(0.2)	748(36)		112766.096	2.3(0.2)	267(18)
	110612.158	3.2(0.3)	516(38)	G133.94+01.06	112160.616	4.2(0.9)	384(63)
	112771.233	4.2(0.9)	326(53)		112760.616	3.2(0.4)	456(47)
G034.39+00.22	106893.082	2.7(0.2)	306(16)	G168.06+00.82	106127.106	6.6(1.0)	474(57)
	110596.233	1.4(0.5)	148(22)		107127.055	8.8(1.3)	550(69)
	110598.904	3.0(0.1)	764(30)	G176.51+00.20	106920.205	2.0(0.4)	54(8)
	110600.548	2.7(0.2)	416(29)		110572.260	1.9(0.3)	88(12)
G035.02+00.34	110005.137	1.9(0.9)	51(23)		110574.829	2.0(0.1)	377(13)
	110595.000	1.7(0.7)	38(16)		110576.541	2.0(0.1)	225(13)
	110597.466	2.7(0.3)	233(19)	G183.72-03.66	110578.596	1.1(0.1)	97(72)
	110599.315	2.3(0.4)	110(17)		110581.164	2.0(0.1)	448(11)
	112791.712	3.6(0.3)	303(24)		110582.877	1.7(0.1)	248(10)
					112775.685	1.3(0.2)	104(14)

Table 6. (Continued)

Sources	ν_{obs} (MHz)	ΔV (km s^{-1})	$\int T_{\text{mb}} dv$ (mK km s^{-1})	Sources	ν_{obs} (MHz)	ΔV (km s^{-1})	$\int T_{\text{mb}} dv$ (mK km s^{-1})
G035.19-00.74	106901.575	3.7(0.2)	486(26)	G188.94+00.88	106912.466	3.0(0.3)	214(20)
	110588.921	2.6(0.3)	284(32)		110578.596	1.6(0.5)	133(18)
	110591.593	3.3(0.2)	1051(43)		110581.336	2.3(0.5)	749(18)
	110593.373	3.2(0.3)	624(45)		110583.048	2.2(0.5)	437(18)
	112785.959	4.0(0.4)	848(63)		112775.856	2.4(0.4)	177(27)
	112794.589	6.8(1.6)	384(82)	G192.60-00.04	105926.798	6.9(0.8)	273(30)
G035.20-01.73	110594.983	9.6(1.1)	644(17)		106539.726	6.0(0.6)	274(23)
G037.43+01.51	110594.589	2.5(0.5)	482(12)		110582.534	1.9(0.2)	194(23)
	110596.439	1.9(0.5)	227(12)		110584.247	1.5(0.1)	105(21)
G043.16+00.01	106910.788	12.3(1.4)	320(39)		111621.233	1.2(0.5)	1054(64)
	107249.246	17.5(2.2)	603(45)		111622.260	1.9(0.5)	2766(64)
	112776.884	5.4(1.4)	297(73)		112777.055	1.3(0.5)	139(45)
	112779.281	4.4(1.1)	314(73)	G209.00-19.38	111932.877	9.7(3.7)	162(60)
G043.79-00.12	110595.000	9.6(1.0)	485(44)		112777.226	2.2(0.9)	117(43)
	112789.041	4.5(0.5)	404(37)	G232.62+00.99	110585.103	2.1(0.3)	154(17)
	112791.712	4.2(1.6)	124(38)		110586.815	2.6(0.3)	153(18)
					112779.623	1.5(0.7)	98(31)
					112796.062	6.3(2.4)	210(61)

Table 7. The detection rate of the related molecules

Section	The related molecules with their detection rates
Sect. 4.2.1	SO (100%), CCS (92%), OCS (96%), SO ₂ (42%)
Sect. 4.2.2	CH ₃ OH (100%), CH ₃ CHO (86%), CH ₃ OCHO (64%), CH ₃ OCH ₃ (70%), C ₂ H ₅ OH (24%), CH ₃ COCH ₃ (10%)
Sect. 4.2.3	HCOOH (72%), CH ₃ COOH (6%)
Sect. 4.2.4	HNCO (86%), NH ₂ CHO (50%)
Sect. 4.2.5	HC ₃ N (100%), HC ₅ N(58%)
Sect. 4.2.6	CN (100%), CH ₃ CN (98%), C ₂ H ₃ CN (32%), C ₂ H ₅ CN (40%)

Table 8. Detected SO, CCS, OCS, and SO₂ summary.

Source	SO	CCS	OCS	SO ₂	Source	SO	CCS	OCS	SO ₂
G000.67-00.03	✓	✓	✓	✓	G035.20-01.73	✓	✓	✓	×
G005.88-00.39	✓	✓	✓	✓	G037.43+01.51	✓	✓	✓	✓
G009.62+00.19	✓	✓	✓	×	G043.16+00.01	✓	✓	✓	✓
G010.47+00.02	✓	✓	✓	✓	G043.79-00.12	✓	✓	✓	✓
G010.62-00.38	✓	✓	✓	✓	G049.48-00.36	✓	✓	✓	✓
G011.49-01.48	✓	×	×	×	G049.48-00.38	✓	✓	✓	✓
G011.91-00.61	✓	✓	✓	×	G059.78+00.06	✓	✓	✓	×
G012.80-00.20	✓	✓	✓	×	G069.54-00.97	✓	✓	✓	✓
G012.88+00.48	✓	✓	✓	✓	G075.76+00.33	✓	✓	✓	×
G012.90-00.24	✓	×	✓	×	G078.12+03.63	✓	✓	✓	×
G012.90-00.26	✓	×	✓	✓	G081.75+00.59	✓	✓	✓	×
G014.33-00.64	✓	✓	✓	×	G081.87+00.78	✓	✓	✓	✓
G015.03-00.67	✓	✓	✓	×	G092.67+03.07	✓	✓	✓	×
G016.58-00.05	✓	✓	✓	×	G109.87+02.11	✓	✓	✓	✓
G023.00-00.41	✓	✓	✓	×	G111.54+00.77	✓	✓	✓	✓
G023.44-00.18	✓	✓	✓	×	G121.29+00.65	✓	✓	✓	✓
G027.36-00.16	✓	✓	✓	×	G123.06-06.30	✓	✓	✓	×
G028.86+00.06	✓	✓	✓	✓	G133.94+01.06	✓	✓	✓	✓
G029.95-00.01	✓	✓	✓	×	G168.06+00.82	✓	×	×	×
G031.28+00.06	✓	✓	✓	×	G176.51+00.20	✓	✓	✓	×
G031.58+00.07	✓	✓	✓	×	G183.72-03.66	✓	✓	✓	×
G032.04+00.05	✓	✓	✓	×	G188.94+00.88	✓	✓	✓	×
G034.39+00.22	✓	✓	✓	×	G192.60-00.04	✓	✓	✓	✓
G035.02+00.34	✓	✓	✓	×	G209.00-19.38	✓	✓	✓	✓
G035.19-00.74	✓	✓	✓	✓	G232.62+00.99	✓	✓	✓	×

Note. ✓ and × represent detection and non-detection for molecules, respectively.

Table 9. Detected CH_3OH , CH_3CHO , CH_3OCHO , CH_3OCH_3 , $\text{C}_2\text{H}_5\text{OH}$, and CH_3COCH_3 summary.

Source	CH_3OH	CH_3CHO	CH_3OCHO	CH_3OCH_3	$\text{C}_2\text{H}_5\text{OH}$	CH_3COCH_3
G000.67–00.03	✓	✓	✓	✓	✓	×
G005.88–00.39	✓	×	✓	✓	×	×
G009.62+00.19	✓	✓	✓	✓	✓	×
G010.47+00.02	✓	✓	✓	✓	✓	✓
G010.62–00.38	✓	✓	✓	✓	✓	×
G011.49–01.48	✓	×	×	✓	×	×
G011.91–00.61	✓	✓	✓	×	×	×
G012.80–00.20	✓	✓	×	✓	×	×
G012.88+00.48	✓	✓	✓	✓	✓	×
G012.90–00.24	✓	×	×	×	×	×
G012.90–00.26	✓	✓	✓	✓	×	×
G014.33–00.64	✓	✓	✓	✓	×	×
G015.03–00.67	✓	×	×	×	×	×
G016.58–00.05	✓	✓	✓	✓	×	×
G023.00–00.41	✓	✓	✓	✓	×	×
G023.44–00.18	✓	✓	✓	✓	×	×
G027.36–00.16	✓	✓	✓	✓	✓	✓
G028.86+00.06	✓	✓	×	✓	×	×
G029.95–00.01	✓	✓	✓	✓	×	×
G031.28+00.06	✓	✓	✓	✓	×	×
G031.58+00.07	✓	✓	✓	✓	×	×
G032.04+00.05	✓	✓	✓	✓	×	×
G034.39+00.22	✓	✓	✓	✓	×	×
G035.02+00.34	✓	✓	×	×	×	×
G035.19–00.74	✓	✓	✓	✓	×	×
G035.20–01.73	✓	✓	×	×	×	×
G037.43+01.51	✓	✓	✓	✓	×	×
G043.16+00.01	✓	✓	✓	✓	×	×
G043.79–00.12	✓	✓	✓	✓	×	×
G049.48–00.36	✓	✓	✓	✓	✓	✓
G049.48–00.38	✓	✓	✓	✓	✓	✓
G059.78+00.06	✓	✓	×	×	×	×
G069.54–00.97	✓	✓	✓	✓	×	×
G075.76+00.33	✓	✓	×	×	✓	×
G078.12+03.63	✓	×	×	×	×	×
G081.75+00.59	✓	✓	×	×	×	×
G081.87+00.78	✓	✓	✓	✓	✓	×
G092.67+03.07	✓	✓	×	✓	×	×
G109.87+02.11	✓	✓	×	×	×	×
G111.54+00.77	✓	✓	✓	✓	✓	×
G121.29+00.65	✓	✓	✓	×	×	×
G123.06–06.30	✓	✓	✓	✓	×	×
G133.94+01.06	✓	✓	✓	✓	×	×
G168.06+00.82	✓	×	×	×	×	×
G176.51+00.20	✓	✓	×	✓	×	×
G183.72–03.66	✓	✓	×	✓	×	×
G188.94+00.88	✓	✓	×	×	×	×
G192.60–00.04	✓	✓	✓	×	✓	×
G209.00–19.38	✓	✓	✓	✓	×	×
G232.62+00.99	✓	×	×	×	×	×

Note. ✓ and × represent detection and non-detection for molecules, respectively.

Table 10. Detected HCOOH and CH₃COOH summary.

Sources	HCOOH	CH ₃ COOH	Sources	HCOOH	CH ₃ COOH
G000.67−00.03	✓	×	G037.43+01.51	✓	×
G009.62+00.19	✓	×	G043.16+00.01	✓	×
G010.47+00.02	✓	✓	G043.79−00.12	✓	×
G010.62−00.38	✓	×	G049.48−00.36	✓	✓
G011.91−00.61	✓	×	G049.48−00.38	✓	✓
G012.80−00.20	✓	×	G059.78+00.06	✓	×
G012.88+00.48	✓	×	G069.54−00.97	✓	×
G014.33−00.64	✓	×	G075.76+00.33	✓	×
G023.44−00.18	✓	×	G081.75+00.59	✓	×
G027.36−00.16	✓	×	G081.87+00.78	✓	×
G028.86+00.06	✓	×	G092.67+03.07	✓	×
G029.95−00.01	✓	×	G109.87+02.11	✓	×
G031.28+00.06	✓	×	G111.54+00.77	✓	×
G032.04+00.05	✓	×	G121.29+00.65	✓	×
G034.39+00.22	✓	×	G123.06−06.30	✓	×
G035.02+00.34	✓	×	G133.94+01.06	✓	×
G035.19−00.74	✓	×	G188.94+00.88	✓	×
G035.20−01.73	✓	×	G192.60−00.04	✓	×

Note. ✓ and × represent detection and non-detection for molecules, respectively.

Table 11. Detected HNCO and NH₂CHO summary.

Sources	HNCO	NH ₂ CHO	Sources	HNCO	NH ₂ CHO
G000.67−00.03	✓	✓	G035.02+00.34	✓	×
G005.88−00.39	✓	×	G035.19−00.74	✓	✓
G009.62+00.19	✓	✓	G035.20−01.73	✓	×
G010.47+00.02	✓	✓	G037.43+01.51	✓	×
G010.62−00.38	×	✓	G043.16+00.01	✓	×
G011.91−00.61	✓	✓	G043.79−00.12	✓	✓
G012.80−00.20	✓	✓	G049.48−00.36	✓	✓
G012.88+00.48	✓	✓	G049.48−00.38	✓	✓
G012.90−00.24	✓	×	G059.78+00.06	✓	×
G012.90−00.26	✓	✓	G069.54−00.97	✓	×
G014.33−00.64	✓	✓	G078.12+03.63	✓	✓
G015.03−00.67	✓	×	G081.75+00.59	✓	×
G016.58−00.05	✓	×	G081.87+00.78	✓	✓
G023.00−00.41	✓	✓	G092.67+03.07	✓	×
G023.44−00.18	✓	✓	G109.87+02.11	✓	×
G027.36−00.16	✓	✓	G111.54+00.77	✓	✓
G028.86+00.06	✓	✓	G121.29+00.65	✓	×
G029.95−00.01	✓	✓	G123.06−06.30	✓	×
G031.28+00.06	✓	✓	G133.94+01.06	✓	×
G031.58+00.07	✓	×	G192.60−00.04	✓	✓
G032.04+00.05	✓	✓	G209.00−19.38	✓	×
G034.39+00.22	✓	✓	G232.62+00.99	✓	×

Note. ✓ and × represent detection and non-detection for molecules, respectively.

Table 12. Detected HC₃N and HC₅N summary.

Sources	HC ₃ N	HC ₅ N	Sources	HC ₃ N	HC ₅ N
G000.67−00.03	✓	✓	G035.20−01.73	✓	×
G005.88−00.39	✓	✓	G037.43+01.51	✓	✓
G009.62+00.19	✓	✓	G043.16+00.01	✓	×
G010.47+00.02	✓	✓	G043.79−00.12	✓	×
G010.62−00.38	✓	✓	G049.48−00.36	✓	✓
G011.49−01.48	✓	×	G049.48−00.38	✓	✓
G011.91−00.61	✓	✓	G059.78+00.06	✓	✓
G012.80−00.20	✓	✓	G069.54−00.97	✓	✓
G012.88+00.48	✓	✓	G075.76+00.33	✓	✓
G012.90−00.24	✓	×	G078.12+03.63	✓	×
G012.90−00.26	✓	×	G081.75+00.59	✓	✓
G014.33−00.64	✓	✓	G081.87+00.78	✓	×
G015.03−00.67	✓	✓	G092.67+03.07	✓	×
G016.58−00.05	✓	×	G109.87+02.11	✓	✓
G023.00−00.41	✓	✓	G111.54+00.77	✓	×
G023.44−00.18	✓	×	G121.29+00.65	✓	✓
G027.36−00.16	✓	✓	G123.06−06.30	✓	✓
G028.86+00.06	✓	✓	G133.94+01.06	✓	×
G029.95−00.01	✓	✓	G168.06+00.82	✓	×
G031.28+00.06	✓	×	G176.51+00.20	✓	×
G031.58+00.07	✓	✓	G183.72−03.66	✓	×
G032.04+00.05	✓	✓	G188.94+00.88	✓	×
G034.39+00.22	✓	✓	G192.60−00.04	✓	×
G035.02+00.34	✓	✓	G209.00−19.38	✓	×
G035.19−00.74	✓	✓	G232.62+00.99	✓	×

Note. ✓ and × represent detection and non-detection for molecules, respectively.

Table 13. Detected CN, CH₃CN, C₂H₃CN and C₂H₅CN summary.

Sources	CN	CH ₃ CN	C ₂ H ₃ CN	C ₂ H ₅ CN	Sources	CN	CH ₃ CN	C ₂ H ₃ CN	C ₂ H ₅ CN
G000.67–00.03	✓	✓	✓	✓	G035.20–01.73	✓	✓	×	×
G005.88–00.39	✓	✓	✓	×	G037.43+01.51	✓	✓	×	×
G009.62+00.19	✓	✓	✓	✓	G043.16+00.01	✓	✓	×	✓
G010.47+00.02	✓	✓	✓	✓	G043.79–00.12	✓	✓	×	✓
G010.62–00.38	✓	✓	✓	✓	G049.48–00.36	✓	✓	✓	✓
G011.49–01.48	✓	✓	×	×	G049.48–00.38	✓	✓	✓	✓
G011.91–00.61	✓	✓	✓	✓	G059.78+00.06	✓	✓	×	×
G012.80–00.20	✓	✓	✓	×	G069.54–00.97	✓	✓	×	×
G012.88+00.48	✓	✓	✓	✓	G075.76+00.33	✓	✓	×	×
G012.90–00.24	✓	✓	×	×	G078.12+03.63	✓	✓	×	×
G012.90–00.26	✓	✓	×	✓	G081.75+00.59	✓	✓	×	×
G014.33–00.64	✓	✓	×	×	G081.87+00.78	✓	✓	×	✓
G015.03–00.67	✓	✓	×	×	G092.67+03.07	✓	✓	×	×
G016.58–00.05	✓	✓	×	✓	G109.87+02.11	✓	✓	×	×
G023.00–00.41	✓	✓	✓	✓	G111.54+00.77	✓	✓	×	×
G023.44–00.18	✓	✓	×	×	G121.29+00.65	✓	✓	×	×
G027.36–00.16	✓	✓	✓	✓	G123.06–06.30	✓	✓	×	×
G028.86+00.06	✓	✓	✓	✓	G133.94+01.06	✓	✓	×	✓
G029.95–00.01	✓	✓	✓	✓	G168.06+00.82	✓	×	×	×
G031.28+00.06	✓	✓	✓	×	G176.51+00.20	✓	✓	×	×
G031.58+00.07	✓	✓	✓	×	G183.72–03.66	✓	✓	×	×
G032.04+00.05	✓	✓	×	✓	G188.94+00.88	✓	✓	×	×
G034.39+00.22	✓	✓	×	×	G192.60–00.04	✓	✓	×	×
G035.02+00.34	✓	✓	×	×	G209.00–19.38	✓	✓	×	✓
G035.19–00.74	✓	✓	×	×	G232.62+00.99	✓	✓	×	×

Note. ✓ and × represent detection and non-detection for molecules, respectively.

Table 14. Detected HC₃N, SO₂, CH₃CN and C₂H₅CN in vibrational state.

Sources	HC ₃ N	HC ₃ N other	SO ₂	CH ₃ CN	C ₂ H ₅ CN	C ₂ H ₅ CN
	v ₇ =1	vibrational states	v ₂ =1	v ₈ =1	v ₁₂ =1-A	v ₂₀ =1-A
G000.67–00.03	✓	×	×	×	×	×
G005.88–00.39	✓	×	×	×	×	×
G009.62+00.19	✓	×	×	×	×	×
G010.47+00.02	✓	✓	✓	✓	✓	✓
G010.62–00.38	✓	×	×	×	×	×
G011.91–00.61	✓	×	×	×	×	×
G012.88+00.48	✓	×	×	×	×	×
G012.90–00.24	✓	×	×	×	×	×
G012.90–00.26	✓	×	×	×	×	×
G015.03–00.67	✓	×	×	×	×	×
G023.00–00.41	✓	×	×	×	×	×
G027.36–00.16	✓	×	×	×	×	×
G028.86+00.06	✓	×	×	×	×	×
G029.95–00.01	✓	×	×	×	×	×
G043.16+00.01	✓	×	✓	×	×	×
G043.79–00.12	✓	×	×	×	×	×
G049.48–00.36	✓	×	✓	✓	×	×
G049.48–00.38	✓	×	✓	✓	×	×
G078.12+03.63	✓	×	×	×	×	×
G081.87+00.78	✓	×	×	×	×	×
G109.87+02.11	✓	×	×	×	×	×
G111.54+00.77	✓	×	×	×	×	×
G133.94+01.06	✓	×	×	×	×	×
G176.51+00.20	✓	×	×	×	×	×

Note. ✓ and × represent detection and non-detection for molecules, respectively.